МІНІСТЕРСТВО ОСВІТИ І НАУКИ УКРАЇНИ
ДЕРЖАВНИЙ УНІВЕРСИТЕТ «КИЇВСЬКИЙ АВІАЦІЙНИЙ ІНСТИТУТ»
ФАКУЛЬТЕТ АЕРОНАВІГАЦІЇ, ЕЛЕКТРОНІКИ ТА ТЕЛЕКОМУНІКАЦІЙ
КАФЕДРА АВІОНІКИ ТА СИСТЕМ УПРАВЛІННЯ

ДОПУСТИТИ ДО ЗАХИСТУ
Завідувач кафедри
_____Олена ТАЧИНІНА
“___” _____ 2025 р.

КВАЛІФІКАЦІЙНА РОБОТА

(ПОЯСНЮВАЛЬНА ЗАПИСКА)
ВИПУСКНИКА ОСВІТНЬОГО СТУПЕНЯ
«БАКАЛАВР»

Тема: **“Оцінювання компонентів зміщення нуля гіроскопів основаних на мікроелектромеханічних системах”**

Виконавець: студент групи Ба-151-21-2-СУ Софія Мельниченко

Керівник: д.т.н., професор Валерій Чіковані

Нормоконтролер: к.т.н., доцент Микола Дивнич

Київ 2025 р.

MINISTRY OF EDUCATION AND SCIENCE OF UKRAINE
STATE UNIVERSITY "KYIV AVIATION INSTITUTE"
FACULTY OF AERONAVIGATION, ELECTRONICS AND TELECOMMUNICATIONS
DEPARTMENT OF AVIONICS AND CONTROL SYSTEMS

APPROVED FOR DEFENCE
Head of the Department
_____ Olena TACHYNINA
"___" _____ 2025

QUALIFICATION PAPER

(EXPLANATORY NOTE)
FOR THE ACADEMIC DEGREE OF BACHELOR

Title: **"Estimation of bias components for gyroscopes based on micro-electro-mechanical systems"**

Submitted by: student of group Ba-151-21-2-СУ Sofiia Melnychenko

Supervisor: DSc, Professor Valerii Chikovani

Standards inspector: PhD, associate professor Mykola Dyvnych

Kyiv 2025

ДЕРЖАВНИЙ УНІВЕРСИТЕТ «КИЇВСЬКИЙ АВІАЦІЙНИЙ ІНСТИТУТ»

Факультет аеронавігації, електроніки та телекомунікацій

Кафедра авіоніки та систем управління

Спеціальність 151 «Автоматизація та комп’ютерно-інтегровані технології»

ЗАТВЕРДЖУЮ

Завідувач кафедри

_____ Олена ТАЧИНІНА

“___” _____2025 р.

ЗАВДАННЯ

на виконання кваліфікаційної роботи

Мельниченко Софії Володимирівни

1. Тема кваліфікаційної роботи: “Оцінювання компонентів зміщення нуля гіроскопів основаних на мікроелектромеханічних системах”
затверджена наказом ректора від “20” березня 2025 р. № 429/ст.
2. Термін виконання роботи: з 19.05.25 по 14.06.2025
3. Вихідні дані для роботи:
Технічні характеристики MEMS-гіроскопа ADIS-16488,
методи моделювання, інструменти MATLAB, дані статичних
вимірювань по осі X.
4. Зміст пояснювальної записки:
Огляд MEMS-гіроскопів, аналіз джерел зсуву, огляд методів
оцінювання, застосування дисперсії Аллана, моделювання в MATLAB,
результати експериментів, висновки.
5. Перелік ілюстративного матеріалу презентації:
Схема принципу роботи, діаграма класифікації гіроскопів, схема методу дисперсії Аллана, графік залежності зсуву від температури, крива дисперсії Аллана, підсумкова таблиця параметрів шуму, приклад коду MATLAB.

6. Календарний план-графік

№	Завдання	Термін виконання	Відмітка про виконання
1	Комплексний огляд наукової літератури з тематики MEMS-гіроскопів	19.05.2025	
2	Ідентифікація та класифікація складових зсуву в MEMS-гіроскопах	23.05.2025	
3	Формулювання математичних моделей для оцінювання зсуву	28.06.2025	
4	Написання першого та другого розділів роботи	02.06.2025	
5	Розробка програми для обчислення дисперсії Аллана та оцінювання трьох перших параметрів зсуву за даними вимірювань	06.06.2025	
6	Оформлення дипломної роботи	10.06.2025	
7	Підготовка презентації	13.06.2025	

7. Дата видачі завдання: 05. 05. 2025

Керівник кваліфікаційної роботи _____ Валерій Чіковані

(підпис керівника)

Завдання прийняв до виконання: _____ Софія Мельниченко

(підпис випускника)

STATE UNIVERSITY “KYIV AVIATION INSTITUTE”

Faculty of aeronautics, electronics and telecommunications

Department of avionics and control systems

Specialty 151 “Automation and computer-integrated technologies”

APPROVED BY

Head of the Department

_____ Olena TACHYNINA

“___” _____2025

QUALIFICATION PAPER ASSIGNMENT FOR GRADUATE STUDENT

Melnychenko Sofiia Volodymyrivna

1. The qualification paper title “Estimation of bias components for gyroscopes based on micro-electro-mechanical systems” was approved by the rector’s order of March 20, 2025 № 429/ст.

2. The paper to be completed between: 19.05.2025 and 14.06.2025

3. Initial data for the paper:
Specifications of the ADIS-16488 MEMS gyroscope, literature on bias and noise modelling, MATLAB tools, and static measurement data from the X-axis.

4. The content of the explanatory note:
Introduction, overview of MEMS gyroscopes, analysis of bias sources, application of Allan variance, MATLAB simulation, experimental results, and conclusions.

5. The list of mandatory illustrations:
Operating principal diagram, gyroscope classification chart, Allan variance method schematic, bias vs. temperature graph, Allan deviation curve, summary table of noise parameters, and MATLAB code example.

6. Timetable

#	Assignment	Dates of completion	Completion mark
1	Comprehensive review of scientific literature on MEMS gyroscope technology	19.05.2025	
2	Identification and classification of bias components in MEMS gyroscopes	23.05.2025	
3	Formulation of mathematical models for bias estimation	28.06.2025	
4	Writing the first and second chapter of the work	02.06.2025	
5	Develop the program for Allan variance computation and estimation of three first bias parameters by measurement data	06.06.2025	
6	Arrangement of diploma work	10.06.2025	
7	Preparation of the presentation	13.06.2025	

7. Assignment issue date: 05.05.2025

Qualification paper supervisor _____ Valerii Chikovani
(the supervisor's signature)

Issued task accepted _____ Sofiia Melnychenko
(the graduate student's signature)

РЕФЕРАТ

70 сторінок, 26 рисунків, 3 таблиці, 13 джерел

Об’єкт дослідження: MEMS-гіроскопи, що застосовуються в інерціальних навігаційних системах та системах відстеження руху ADIS-16488.

Предмет дослідження: Похибки зсуву у сигналах MEMS-гіроскопів та методи їх ідентифікації, моделювання й оцінювання.

Мета роботи: Проаналізувати та оцінити складові зсуву в MEMS-гіроскопах за допомогою математичного моделювання та аналізу дисперсії Аллана.

Методи дослідження: Теоретичний аналіз, огляд літературних джерел, математичне моделювання, статистичний аналіз із використанням дисперсії Аллана, моделювання в MATLAB.

У роботі здійснено оцінювання параметрів шуму на основі реальних даних з гіроскопа ADIS-16488. Отримані результати є актуальними для вдосконалення автономних навігаційних систем.

Ключові слова: MEMS-ГІРОСКОПИ, ЗСУВ, ДИСПЕРСІЯ АЛЛАНА, ІНЕРЦІАЛЬНІ СЕНСОРИ, НЕСТАБІЛЬНІСТЬ ЗСУВУ, MATLAB.

ABSTRACT

70 pages, 26 figures, 3 tables, 13 references

Object of research: MEMS gyroscopes used in inertial navigation and motion tracking systems ADIS-16488.

Subject of the research: Bias error in MEMS gyroscope signals and methods for its identification, modelling, and estimation.

Purpose of the work: Analyse and estimate the bias components in MEMS gyroscopes using mathematical modelling and Allan variance analysis.

Research methods: Theoretical analysis, literature review, mathematical modelling, statistical analysis using Allan variance, and simulation in MATLAB.

The results include the estimation of noise using real data from the ADIS-16488 gyroscope. The findings are relevant for improving autonomous navigation systems.

Keywords: MEMS GYROSCOPE, BIAS, ALLAN VARIANCE, INERTIAL SENSORS, BIAS INSTABILITY, MATLAB.

TABLE OF CONTENTS

INTRODUCTION

These days, advanced navigation, stabilisation, and motion tracking systems are built on the foundation of angular velocity measurement that is both accurate and repeatable. Micro-electro-mechanical systems (MEMS) gyroscopes have emerged as one of the most prevalent technologies for giving such measurements due to their compact size, minimal power consumption, and ease of integration into embedded systems. Microelectromechanical system gyroscopes are utilised in several technologies, including cell phones, drones, aerospace platforms, and autonomous vehicles.

While beneficial, MEMS gyroscopes are susceptible to several defects that may undermine the accuracy of their measurements. Bias, manifesting as a non-zero output despite the gyroscope being stationary, is a significant contributor to inaccuracy. Inertial navigation systems and integrated motion estimation algorithms lack precision due to bias, temporal instability, and temperature sensitivity. Prolonged neglect of bias may result in significant drift and accumulation of positional inaccuracies.

The increasing demand for cost-effective, high-performance inertial sensors—particularly in systems dependent on prolonged or highly accurate orientation data—renders efficient bias estimation and correction algorithms essential. Conventional calibration methods are either inadequate or impractical in dynamic situations. Novel methodologies rely on statistical tools to analyse and quantify bias behaviour from the sensor's output data in controlled or operational environments.

This dissertation uses the Allan variance approach, a reliable time-domain analytical tool, to predict the bias components in MEMS gyroscopes. This method enables us to differentiate various types of noise and errors in the output of inertial sensors. This technique employs a static MEMS gyroscope to measure critical variables such as bias instability, angle random walk, and other stochastic processes affecting the sensor.

This work's significant practical contribution is the enhancement of the precision and reliability of MEMS gyroscope measurements using simulation-based analysis. The research illustrates that Allan variance curves can be utilised for theoretical comprehension as well as for bias characterisation and system calibration by constructing a model in the MATLAB environment. Any sector reliant on inertial sensing and utilising MEMS gyroscopes will benefit from the results of this research. This encompasses mobile technology, aviation, defence, and robotics.

Relevance of the work. MEMS gyroscopes are widely used for navigation and motion tracking due to their compact size and low cost. However, bias causes errors even when the sensor is stationary, reducing accuracy.

In systems like drones and aircraft, where GNSS may be unavailable, bias leads to significant drift. Estimating and correcting this bias is essential.

This work applies Allan variance analysis to identify bias components in the ADIS-16488 MEMS gyroscope, improving the precision and stability of inertial systems.

Objectives of the work. To achieve the stated aim, the following objectives were set:

- To study the physical and functional principles of MEMS gyroscopes and review their main structural types and applications.
- To define the concept of bias in MEMS gyroscopes and analyse the internal and external factors that affect it.
- To examine various methods for estimating MEMS gyro bias, with a particular focus on Allan variance.
- To develop a mathematical and simulation model for analysing MEMS gyro output in a static environment.
- To apply Allan variance analysis to identify and quantify key bias components such as bias instability and angle random walk.
- To interpret the results and assess the suitability of the selected method for characterising MEMS gyro performance.

Subject of research. The subject of research is the bias error in MEMS gyroscope signals and the methods for its identification, modelling, and estimation using time-domain statistical techniques.

Scientific Novelty. The novelty of this work lies in the integration of Allan variance-based analysis for identifying multiple bias components in MEMS gyroscope data, with a focus on its use in static modelling scenarios. The work demonstrates how the Allan variance curve can be used not only for bias estimation but also for classification of different noise types, which is critical for improving inertial sensor performance.

Practical Significance. The outcomes of this research can be applied to real-world tasks such as calibration, signal correction, and performance assessment of MEMS gyroscopes in navigation systems, robotics, UAVs, and wearable devices. The developed methodology offers a cost-effective approach for improving measurement accuracy without requiring expensive hardware modifications.

Structure of the Thesis. The thesis consists of three main chapters and supporting materials:

- Chapter 1 provides an overview of MEMS gyroscopes, their types, manufacturing technologies, major producers, and application domains.
- Chapter 2 explores the concept of MEMS gyro bias, its sources, behaviours over time and temperature, and mathematical models.
- Chapter 3 presents the Allan variance method for bias estimation, the breakdown of noise components in MEMS gyro signals, and interpretation of simulation results.

The work concludes with final remarks, a list of references, and appendix containing additional figures and MATLAB implementation scripts.

CHAPTER 1 GYROSCOPES BASED ON MICRO-ELECTRO-MECHANICAL SYSTEMS (MEMS)

1.1 Overview of MEMS Gyroscopes

Micro-Electro-Mechanical Systems (MEMS) gyroscopes are compact, low-cost inertial sensors that detect angular velocity. These devices belong to a broader family of gyroscopes, which are generally categorised by their actuation and sensing methods: mechanical, optical, or atomic. While traditional mechanical gyroscopes rely on momentum conservation using spinning masses, and optical gyroscopes use the Sagnac effect to detect angular movement via interference of light, MEMS gyroscopes employ vibrating structures that react to angular motion through the Coriolis effect.

MEMS gyroscopes fall under the category of mechanical gyroscopes but are unique in that they use vibrating microstructures instead of large spinning wheels. The Coriolis force generated by these vibrations under rotation allows the sensor to measure angular velocity. A typical MEMS gyroscope uses capacitance sensing or piezoelectric detection to monitor the displacement of a vibrating proof mass. The design is favourable for integration into modern electronics due to its compact size, low power consumption, and affordability.

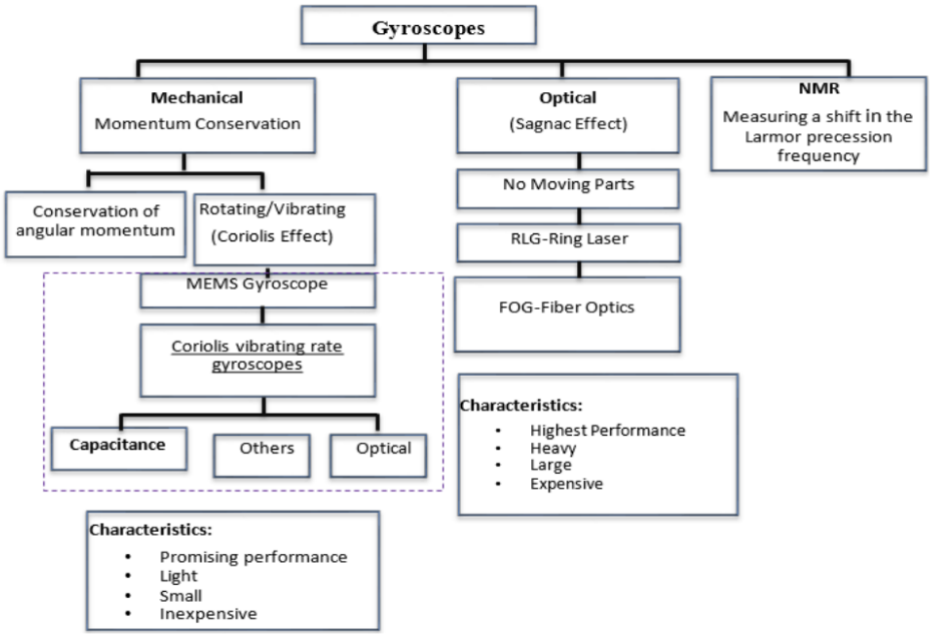

Fig. 1.1 Comparison of Optical vs. Mechanical Gyroscopes.

Figure 1.1 illustrates a classification of gyroscope technologies, showing the differences in structure, sensing mechanisms, and characteristics. While optical gyroscopes (such as RLGs and FOGs) are recognised for their high accuracy and are commonly used in navigation and aerospace systems, MEMS gyroscopes dominate consumer electronics due to their small footprint, scalability, and low production costs.

MEMS vibratory gyroscopes measure angular rotation around specific axes with respect to an inertial reference frame. Their applications are diverse and include rollover detection in vehicles, anti-skid systems, GPS stabilisation, gaming controllers, smartphone motion tracking, camera stabilisation, medical instruments, and drone stabilisation systems. Their versatility and affordability have led to their adoption in nearly all portable electronic devices requiring motion detection.

Despite their advantages, MEMS gyroscopes face performance limitations compared to optical systems. Key issues include Angle Random Walk (ARW), bias instability, and limited bandwidth, which are critical challenges for high-precision and tactical-grade applications. Bias instability leads to errors that accumulate over time, degrading the accuracy of position estimation in inertial navigation systems.

Additionally, MEMS devices are highly sensitive to temperature changes, mechanical stress, and aging effects, all of which can introduce drift in the output.

Research in this field often targets improving these shortcomings, such as through innovative designs like cantilever beam structures, closed-loop architectures, or advanced temperature compensation algorithms. Recent developments also include the use of machine learning techniques to model and correct sensor biases in real-time.

Structurally, MEMS gyroscopes are mainly vibratory devices, often modelled using two degrees of freedom (2-DOF) resonator systems. A typical configuration, shown in Figure 1.2, includes a suspended proof mass held by flexible suspension beams. This configuration allows the mass to oscillate freely within a defined plane. The vibration of the mass is excited along a drive axis, while angular motion about an orthogonal axis induces Coriolis forces that displace the mass along a sense axis. This displacement is detected using sense electrodes arranged around the mass.

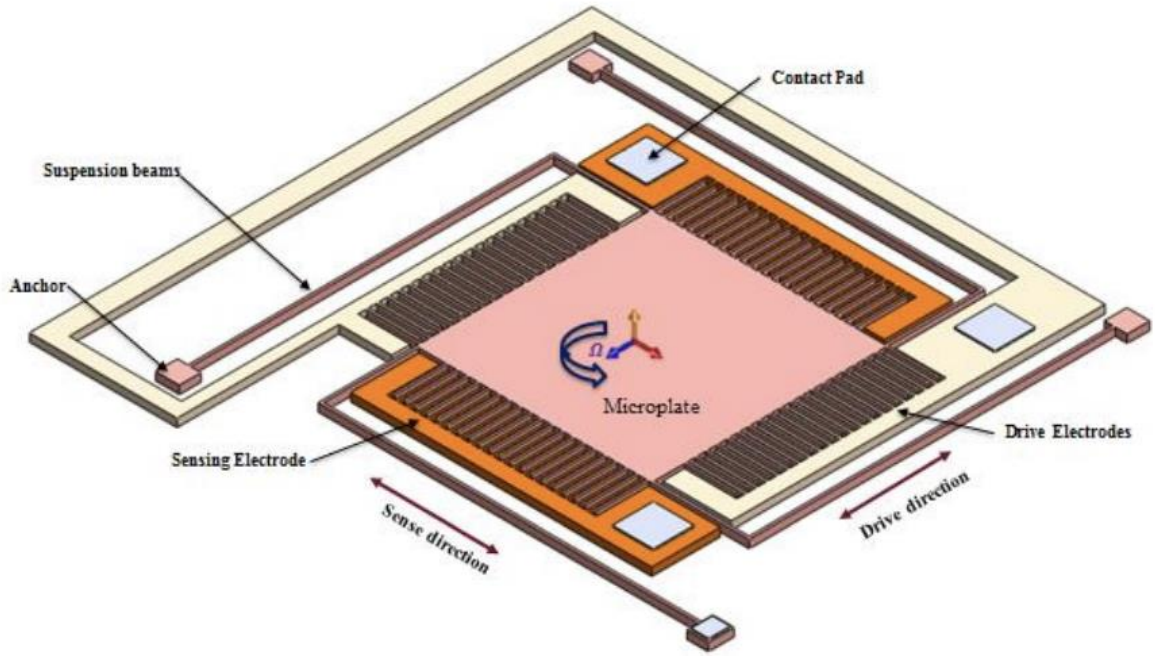

Fig. 1.2 3D Model of Crab-Leg MEMS Gyroscope

The proof mass is driven into resonance along the drive axis using drive electrodes. When the sensor undergoes rotation, a Coriolis force perpendicular to both the drive and rotation axes is generated, inducing displacement along the sense

direction. This movement is typically very small and requires high-precision capacitive sensing for detection. Proper tuning of the resonant frequency is essential for achieving high sensitivity.

The Coriolis force is a function of the vibrating mass, angular speed, and oscillation velocity. For resonance conditions, the driving frequency must match the sensing frequency to maximise sensitivity. Small displacements on the order of 10 μm must be detected, requiring highly sensitive capacitive sensors. Equation (1.1) gives the Coriolis force:

$$\vec{F_c} = -2m(\vec{\Omega} \times \vec{v_d}) \propto 10^{-12} \times 10^{2} \times 10^{-2} \sim pN \quad (1.1)$$

Where:

- $\vec{F_c}$: Coriolis force
- m: mass of the proof mass
- $\vec{\Omega}$: angular velocity
- $\vec{v_d}$: velocity of the driven oscillation

Drive mode oscillations for MEMS gyroscopes typically range from 5 to 40 kHz, with amplitudes of 0.5 to 1.5 μm and peak velocities around 0.06 m/s. These small forces, typically in the pico-Newton range, make sensing a significant engineering challenge. Capacitive sensing techniques with high resolution are employed to detect these subtle changes. Some newer MEMS designs also incorporate piezoresistive or optical sensing to improve detection accuracy.

MEMS gyroscopes offer a balance between performance and practicality, enabling the development of compact and affordable inertial sensing solutions across various industries. As research continues to address performance limitations, the future of MEMS gyroscope technology holds promise for even broader applications, including autonomous navigation, biomedical devices, and space systems.

1.2 Types & Designs of MEMS Gyroscopes

MEMS gyroscopes are not a one-size-fits-all solution; instead, they exist in a variety of types and structural configurations tailored to meet specific functional demands. The working principle in all of them relies on detecting the Coriolis force generated by vibrating microstructures under rotational motion. However, how that vibration is generated, how the resulting motion is sensed, and how the structure is physically designed can differ significantly. These differences affect the gyroscope's sensitivity, noise behaviour, power consumption, temperature stability, and suitability for particular use cases.

One key classification is based on vibration mode — this refers to how the moving structure vibrates in response to actuation. For example, in-plane modes vibrate parallel to the substrate surface, while out-of-plane modes vibrate perpendicularly. Some designs use torsional oscillation, rotating parts instead of translating them linearly. The motion mode directly influences the Coriolis force direction, sensing scheme, and achievable performance.

Another common categorisation is by the number of sensing axes. Basic gyroscopes detect angular velocity around a single axis, while more advanced designs combine multiple sensing elements to form dual- or tri-axis gyroscopes. These are especially useful in modern devices like smartphones and drones, where full 3D motion tracking is essential.

MEMS gyroscopes are also distinguished by their detection mechanisms — how they sense the Coriolis-induced motion. Capacitive sensing is the most widespread due to its CMOS compatibility and low cost, but piezoelectric and piezoresistive approaches also exist, offering better performance in harsh environments. Optical sensing, although rare in MEMS due to fabrication complexity, provides exceptional precision.

Finally, the physical structure of the MEMS sensor — such as the crab-leg, tuning fork, wineglass, or folded beam designs — determines the device's resonance behaviour, frequency stability, and integration feasibility. Each design has specific

advantages and trade-offs, often chosen based on whether the target application values cost-efficiency, ruggedness, or ultra-high sensitivity.

In the following sections, we will examine these classification categories in detail, exploring the most common types of MEMS gyroscope designs and analysing their advantages, limitations, and application areas.

Gimbal Gyroscopes

Gimbal MEMS gyroscopes are inspired by traditional spinning rotor gyroscopes, where a mass is suspended on multiple axes using gimbals to allow free rotation and independent motion sensing. In MEMS systems, a vibrating component is hung inside two or more micro-fabricated gimbals rather than a spinning rotor. Like previous MEMS gyroscopes, these structures have improved multi-axis isolation and dynamic decoupling, allowing them to measure angular velocity by using the Coriolis effect.

Suspended by torsional springs or flexural pivots, the outer gimbal—used for excitation—and inner gimbal—used for sensing—comprise the fundamental structure. Actuation by the outer frame causes the inner component to vibrate at a resonant frequency. The Coriolis force shifts energy from the driving motion to a perpendicular axis when the device rotates, hence causing oscillation of the inner gimbal, which is detected capacitively.

While some systems include electromagnetic coils or piezoelectric components for actuation and readout, others have comb-drive actuators and capacitive sensing electrodes. Often, the mechanical design has torsional bars that preserve the structural alignment of both gimbals even allowing rotational motion.

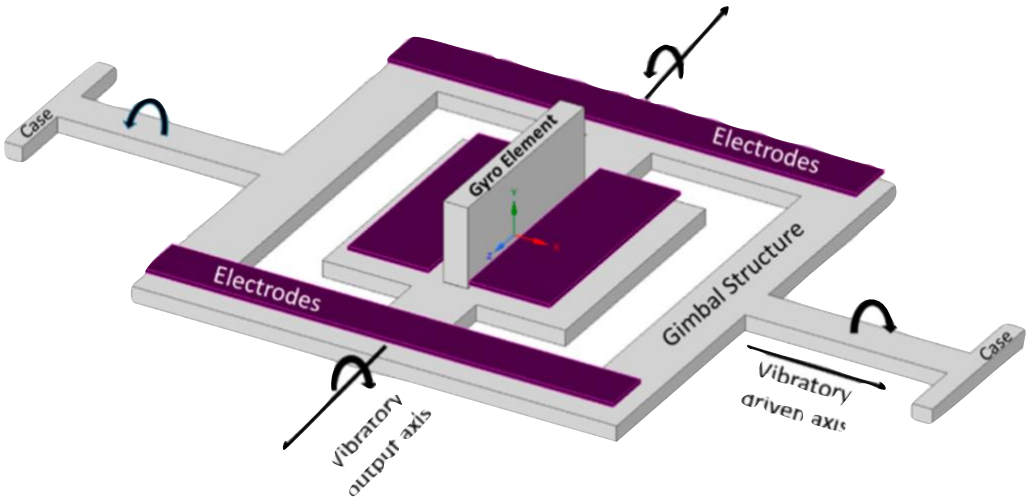

Fig. 1.3 Schematic diagram of a two-gimbal MEMS gyroscope using inner and outer suspended frames.

Various MEMS gimbal gyroscope designs have been created to increase sensitivity, bandwidth, and manufacturing compatibility.

- VWOG (Vibrating Wheel on Gimbal): A circular wheel structure mounted on a gimbal, driven by stator combs and supported by anchored springs. The vibration transfers through the gimbal system and rotation-induced displacement are picked off using sensing electrodes beneath the wheel.
- Dual-Gimbal with Comb Structures: Comb drives create rotational motion in the primary axis, while Coriolis-induced motion activates a secondary oscillator along the sensing axis. This dual-stage motion decouples drive and sense dynamics, improving clarity of signal output.
- Magnetic Coil-Driven Gimbals: Incorporate current-carrying coils for inner gimbal excitation. Rotation causes a response in the outer gimbal, which is monitored via induced voltages.
- Ni–Fe Alloy Gimbals: Address residual stress and buckling issues of pure nickel structures by using Ni–Fe composites, improving structural stability in vertical MEMS designs. (Figure 1.4).
- Geometry Optimisation: Studies show that hexagonal-shaped gimbals offer lower linearity error, while circular structures offer higher scale factors — allowing design trade-offs based on application needs (Figure 1.5).

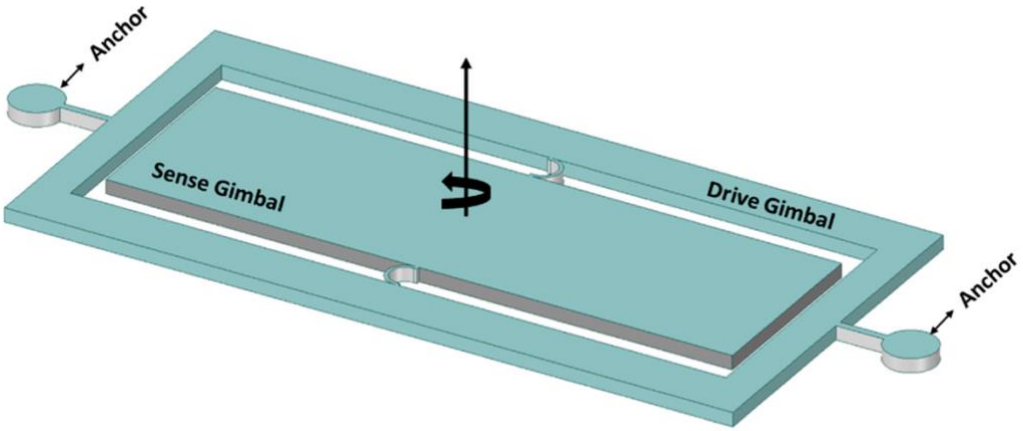

Fig. 1.4 Ni–Fe alloy-based two-gimbal system gyroscope.

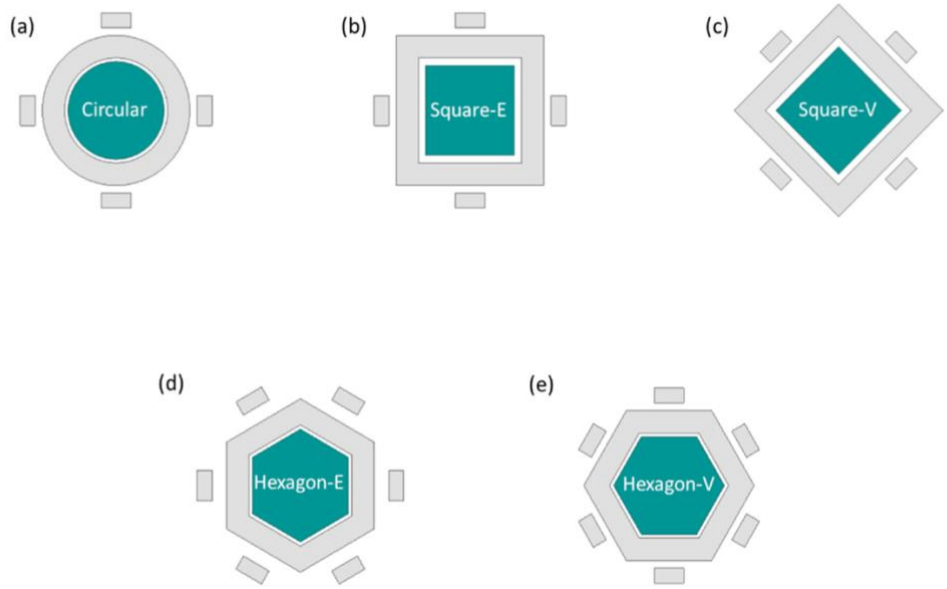

Fig. 1.5 Study of different shapes of an MEMS vibrating wheel on a gimbal gyroscope. (**a**) circular (**b**) square-edge (**c**) square-vertex (**d**) hexagon-edge (**e**) hexagon-vertex.

Structural configuration, material selection, and manufacturing accuracy all have a major impact on gimbal MEMS gyroscope performance. Devices built on dual-gimbal comb architectures have shown:

- ARW as low as $0.14deg/\sqrt{h}$

- Bias instability about 65 deg/h
- Drive and sense frequency separation typically around 1% for optimised resonance
- Depending on actuation/sensing technique, sensitivity varies from 10 to 150 mV/deg/s.
- With best gimbal geometry, linearity error can be reduced.

Although more difficult to manufacture and package than single-axis MEMS gyros, gimbal designs offer improved axis decoupling, multi-axis capability, and vibration rejection, hence appropriate for dynamic settings.

Gimbal MEMS gyroscopes are perfect for:

- Precision instruments and scientific platforms
- Multi-axis inertial measurement units (IMUs)
- Compact systems needing integrated drive/sense separation
- Environments needing lower susceptibility to external vibrations

Their improved mechanical design makes them ideal for usage in military-grade systems, aerospace components, and mobile robotics.

Tuning Fork Gyroscopes (TFGs):

Tuning Fork MEMS Gyroscopes (TFGs) are among the most widely used vibratory gyroscope architectures due to their compact size, simplicity, and compatibility with MEMS fabrication techniques. Oscillating in anti-phase along the drive axis, two symmetric proof masses drive these gyroscopes. The Coriolis effect produces a secondary motion along the sense axis when exposed to external angular velocity perpendicular to this axis; this motion is sensed with capacitive electrodes.

When exposed to external angular velocity perpendicular to this axis, the Coriolis effect causes a secondary motion along the sense axis, which is detected using capacitive electrodes.

Usually, the structure is a symmetrical tuning fork made of two proof masses hung by spring beams. Comb-drive actuators cause the masses to oscillate in-plane;

capacitive sense electrodes are set to identify out-of-plane or lateral movement caused by the Coriolis force. Figure 1.6 illustrates a schematic of this operational concept.

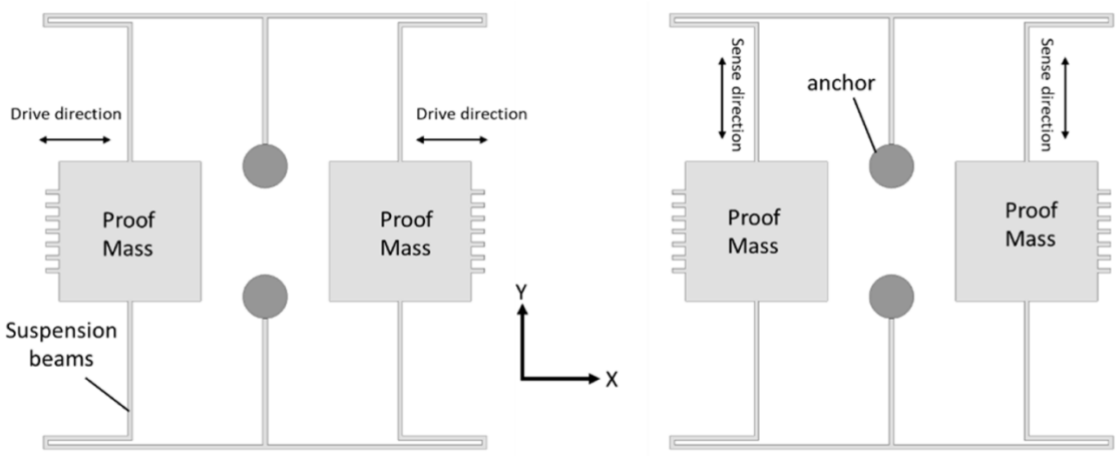

Figure 1.6 Operation of a basic MEMS tuning fork gyroscope.

Differential motion of the proof masses guarantees great sensitivity and common-mode noise suppression. TFGs are perfect for mass production since electrostatic drive and capacitive sensing provide low power use and compatibility with on-chip integration.

Modern TFGs have developed to include various design enhancements: Using SOI wafres and deep reactive-ion etching (DRIE), high-Q symmetric architectures provide outstanding resolution and stability. Improving performance in atmospheric pressure settings by using Z-axis TFGs with freestanding designs to reduce squeeze-film damping. Anchored coupling techniques to raise drive-mode stiffness and enhance frequency separation and linearity. Diamond-anchored or perforated masses to lower mode mismatch and improve thermal response. Sub-micron gaps guarantee structural accuracy and two-mask SOI manufacturing streamlines processing. Figure 1.7 shows a good quality implementation showing mode balancing and precise structural specification.

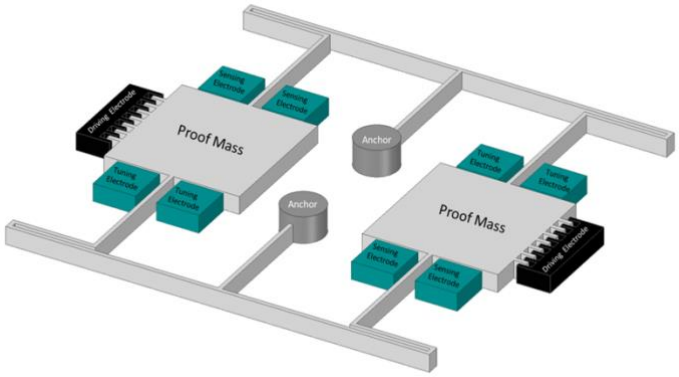

Fig. 1.7 Schematic diagram of high Q MEMS tuning fork gyroscope.

Common in consumer electronics, automotive systems, and drones, TFGs provide a consistent mix of cost and performance. Depending on the design:

- Quality factors (Q): 800 – 80,000
- Bias stability: as low as 0.2 deg/h
- Angle Random Walk (ARW): 0.1 – 1.0 deg/√h
- Sensitivity: typically, 90 – 130 mV/deg/s
- Resonant frequencies: 2 – 10 kHz depending on mass and spring stiffness

Often, closed-loop control systems and advanced signal processing are used to enhance linearity and dynamic range, particularly in inertial navigation applications.

TFGs are commonly used in:

- Automotive rollover detection and ESC systems
- Smartphones and gaming motion sensors
- Consumer and industrial drones
- Camera stabilisation systems
- Inertial Measurement Units (IMUs) for navigation

Many commercial-grade MEMS gyroscope applications still find them a go-to choice because of their established technology, scalable manufacturing, and strong performance.

Vibrating Ring Gyroscopes (VRGs):

A high-performance kind of MEMS gyroscopes, vibrating ring gyroscopes (VRGs) measure angular velocity by means of circular or ring-shaped resonators. Their natural mechanical symmetry and balanced structure give exceptional thermal stability, high Q-factors, and exact frequency matching between drive and sense modes—all of which are vital for sensitive, low-noise angular rate sensing.

All of which are vital for sensitive, low-noise angular rate sensing, their natural mechanical symmetry and balanced structure offer remarkable thermal stability, high Q-factors, and exact frequency matching between drive and sense modes.

Usually eight, a ring hung by several springs linked to a central anchor forms the heart of a VRG (Figure 1.8). This design allows the ring to vibrate in a standing wave pattern inside the plane of the substrate. Electrodes distributed around the ring drive and sense these vibrations via capacitive coupling.

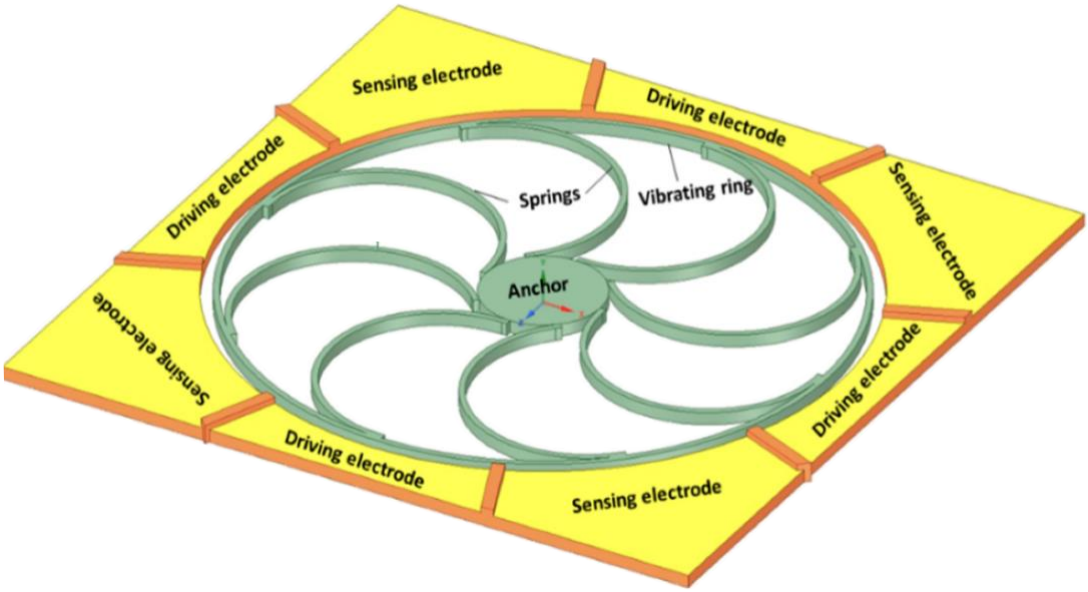

Fig. 1.8 Schematic representation of the basic design of a vibrating ring gyroscope.

Operating the ring uses AC voltage provided to driving electrodes to excite it into a drive mode, often a second-order elliptical mode. Without rotation, the vibration stays in a set pattern. The Coriolis effect creates a second standing wave—the sense

mode—oriented 90° from the driving pattern when external angular velocity is applied, usually around the out-of-plane axis. Capacitive sensing electrodes pick up this caused vibration (Figure 1.9).

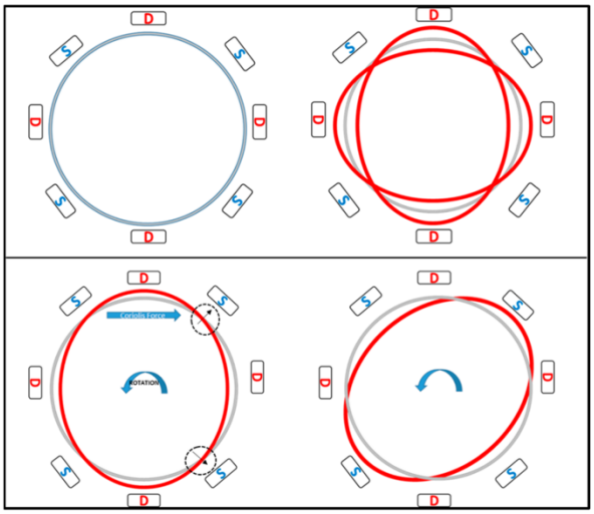

Fig. 1.9 Schematic demonstration of the operation of a vibrating ring gyroscope.

- The closed ring design reduces energy loss, resulting in greater Q-factors.
- Good mode matching: Frequency tuning is simpler, which helps the signal-to-noise ratio.
- Symmetry lowers temperature-induced drift, therefore enhancing thermal stability.
- Less quadrature error: Because of negligible mechanical asymmetries.
- Easily miniaturised and integrated using conventional MEMS techniques, scalability

Energy transfer efficiency and sensitivity depend on the near match between drive and sensing frequencies, often within 10–100 Hz. Some systems allow for frequency mismatch tuning during operation via piezoelectric components or electrostatic softening.

Some designs allow for frequency mismatch tuning during operation via electrostatic softening or piezoelectric components.

Several support systems have been created to increase mechanical dependability and sensitivity:

S-shaped springs help to isolate the ring from the anchor, therefore lowering mechanical stress and enhancing frequency stability.

Commonly seen in atmospheric-pressure gyroscopes with Q-factors between 150 and 200 (Figure 1.10).

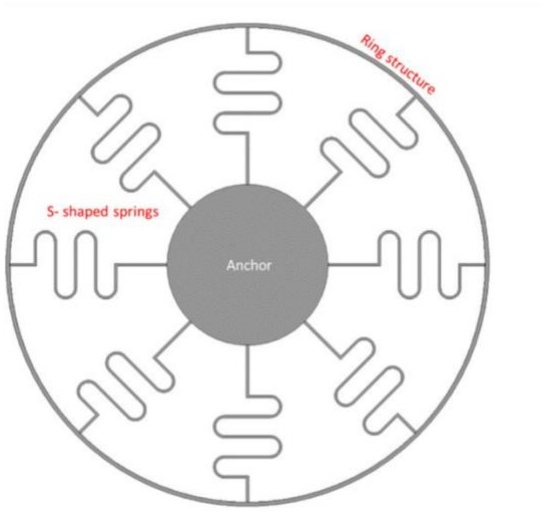

Fig. 1.10 VRG with eight symmetrical S-shaped support springs.

Increase rigidity while preserving flexibility with double U-Beam Supports, therefore strengthening external shock resistance and promoting structural linearity.

Drive/sense frequency separation can be as low as $10-20\text{Hz};\text{ARW}0.7\text{deg}/\sqrt{\text{h}}$(Fig. 1.11).

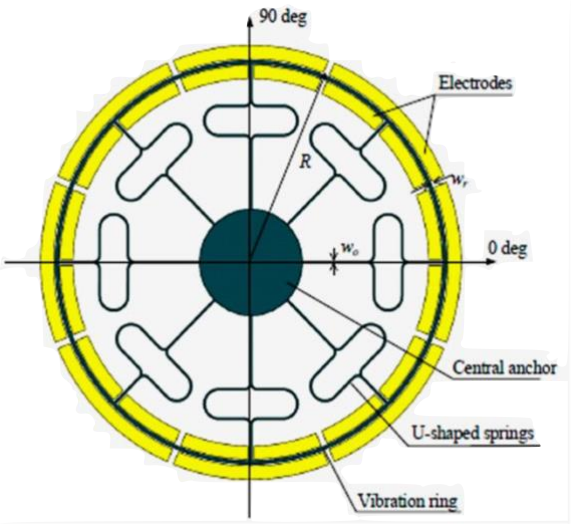

Fig. 1.11 Double U-beam supported VRG for enhanced stability and sensitivity.

Introduce several concentric rings in multi-ring designs to raise effective mass and enhance mechanical gain. These are beneficial for uses needing extremely high sensitivity in a little footprint.

Improvements in sensitivity over single-ring designs of up to 30% have been noted. See Figure 1.12

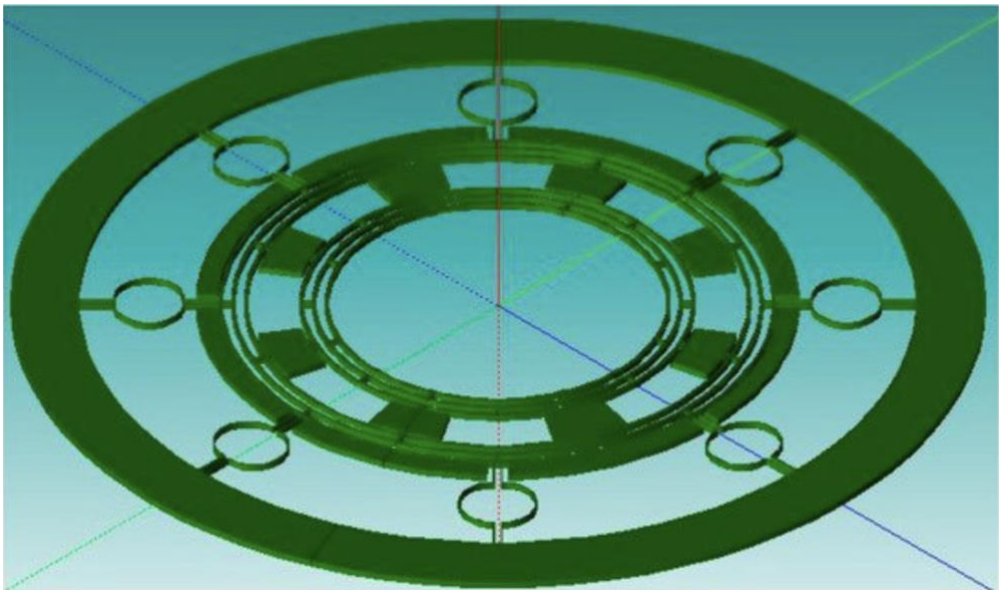

Fig. 1.12 Multi-ring VRG design for improved mechanical gain and signal response

Table 1.1

VRG Performance Features

Parameter	**Typical Value**
Quality Factor (Q)	1,000-12,000 (vacuum-packaged)
Angle Random Walk (ARW)	0.05 and 1.0$deg/\sqrt{h}$
Bias Instability	< 0.01 to a few deg/h
Sensitivity	100 - 150 mV/deg/s (high-end designs)
Resonant Frequency	6 - 40 kHz
Linearity Error	< 0.02%

These characteristics vary depending on fabrication methods (SOI, bulk micro-machining, DRIE), geometry (ring radius, width, and spring design), and packaging (vacuum-sealed or atmospheric). Sometimes, piezoelectric or electrostatic tuning is used to preserve ideal frequency matching over temperature ranges.

Sometimes, piezoelectric or electrostatic tuning is used to preserve ideal frequency matching over temperature ranges.

VRGs are used in:

- Aerospace and satellite inertial navigation
- Tactical-grade military IMUs
- Robotics and high-end industrial systems
- Automotive stability control systems

Their small size and low power use also fit them for future integration into miniaturised navigation solutions and autonomous systems.

Multi-Axis Gyroscopes:

Multi-axis MEMS gyroscopes are designed to detect angular velocity along two or more axes using a single, integrated device. Unlike single-axis gyroscopes, these devices often sense motion in many directions, usually along the x-, y-, and z-axes, using dynamic symmetry and connected oscillators. Especially in modern inertial measurement units (IMUs), where compactness and complete spatial orientation tracking are crucial, they are somewhat common.

A two-dimensional micro-mechanical gyroscope built with four cantilever plates hanging over a substrate is one particularly remarkable illustration. Sensed capacitively, these cantilevers coupled with stationary electrodes react to Coriolis-induced displacements. Sensitivity was much better when the driving and sense frequencies matched; it got to 0.1 mV/deg/s.

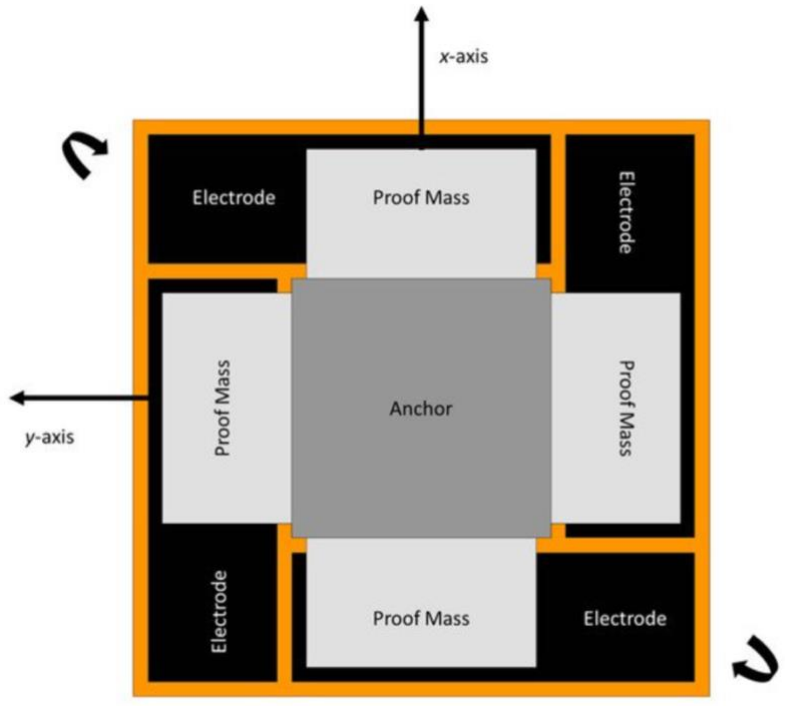

Fig. 1.13 Schematic diagram of a novel two-dimensional micro-machined gyroscope with four cantilevers.

Another method used a dual-axis disk-type MEMS gyroscope consisting of a thin polysilicon disc suspended by four torsional beams. Angular resonance around the z-axis drives the disc; rotation along x or y produces a Coriolis reaction seen on the opposite axis. Though initial angle random walk (ARW) was large and later reduced to $2deg/\sqrt{h}$ with frequency tuning, this symmetric design enables dual-axis detection with strong coupling.

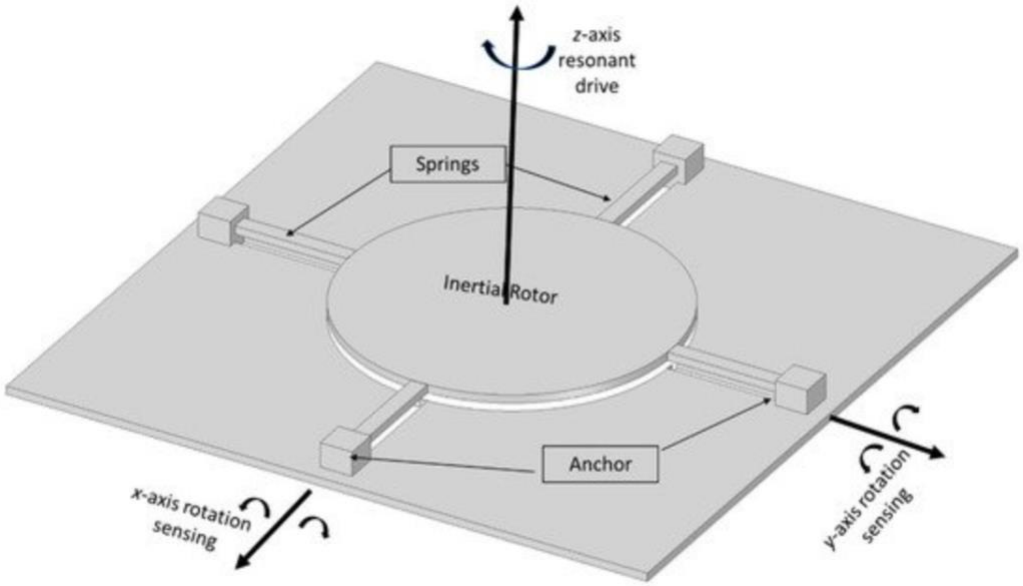

Fig. 1.14 Schematic diagram of a dual-axis micro-machined vibrating gyroscope.

NASA's Jet Propulsion Laboratory created a space-grade micro-machined gyroscope system with an integrated package comprising a preamplifier and signal conditioning. With just a 7 Hz separation between drive and sensing modes, the device ran with a scale factor of 24 mV/deg/s, bias stability of 70 deg/h, and ARW of 6.3 $deg/\sqrt{h}$, stressing the need of exact mode tuning.

Designed as a tunable MEMS gyroscope, it has two hanging plates electrostatically driven in opposing directions. Coriolis-induced motion altered the capacitance between the plates and bottom electrodes, hence allowing dual-axis detection and dynamic tuning.

More recent developments are the four-mass, rate-integrating gyroscope, which has a very symmetric and dynamically balanced vacuum-sealed construction.

Operating at about 2 kHz, these devices have Q-factors over one million. With a 100 Hz bandwidth and very consistent mode matching, their linear response range covers ±450 deg/s.

Using a two-phase locked loop, was created a frequency-modulated four-mass gyroscope with built-in digital control. From -40 °C to 100 °C, it kept remarkable performance throughout a broad temperature range.

Further developments are the twin Foucault pendulum gyroscope, which uses two symmetrical masses vibrating in anti-phase. With Q-factors over 100,000 and an operating frequency of 2.7 kHz, this whole-angle design showed great stability. Over long durations, the approach shows great promise for precise angular rate measurement.

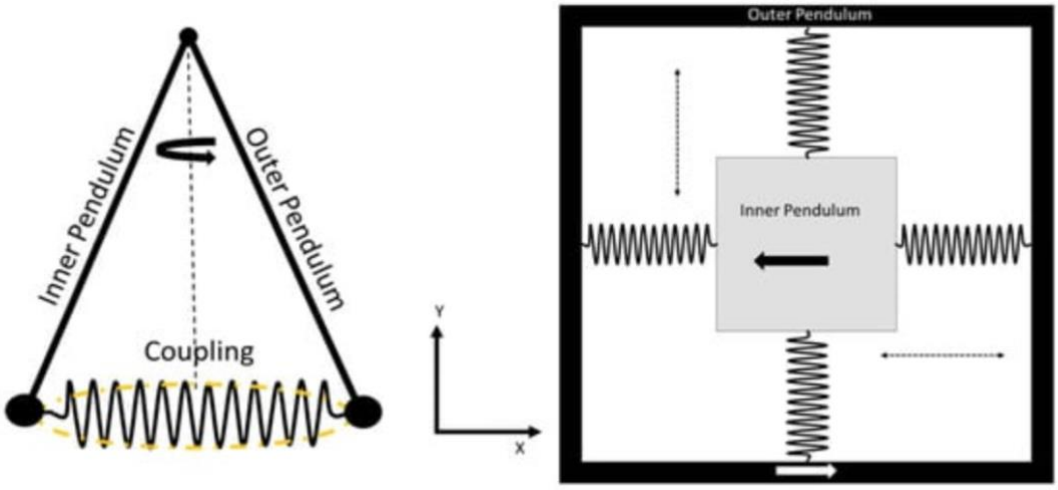

Fig. 1.15 Schematic diagram of a dual Foucault pendulum gyroscope. Two masses vibrate in anti-phase motion.

Three-axis MEMS gyroscopes have been created to achieve complete 3D angular detection. One such device obtained good performance in yaw and pitch detection by means of frequency-modulated outputs using twin structures built on a 24 µm structural layer. These devices showed good axis decoupling and strong scale factor stability.

1.3 Manufacturing Technologies

MEMS gyroscope processing is a type of micro-fabrication technology designed to create structures at the scale of nanometres to millimetres. Generally general, MEMS manufacture combines a great variety of contemporary manufacturing techniques. These techniques can be classified into three primary groups depending on the technology approach:

1. Silicon-based MEMS fabrication, which is derived from semiconductor integrated circuit processing technologies.
2. LIGA (Lithographie, Galvanoformung, Abformung) techniques for high-aspect-ratio microstructures.
3. Ultra-precision mechanical machining, involving fine-scale milling, drilling, and shaping.

This paper focuses on the manufacturing of a MEMS gyroscope using Silicon on Insulator (SOI) technology. A three-layer structure characterises an SOI wafer: the top (device) layer and bottom (handle) layer are both silicon, separated by a buried oxide (BOX) layer of silicon dioxide. SOI wafers are perfect for MEMS gyroscope manufacturing since their customisable thickness and conductivity of every layer, together with minimal internal stress. Consequently, SOI has become the principal material platform for manufacturing MEMS gyroscopes; the SOI process is considered the conventional method in the sector.

MEMS Gyroscope Fabrication Process

The complete MEMS gyroscope fabrication procedure is split into two main phases:

1. Glass substrate processing is the first stage, which entails metal electrode patterning on the glass.
2. Processing of SOI silicon structures, which creates the sensitive components of the gyroscope.

The glass substrate preparation workflow is outlined below and shown in figure 1.16

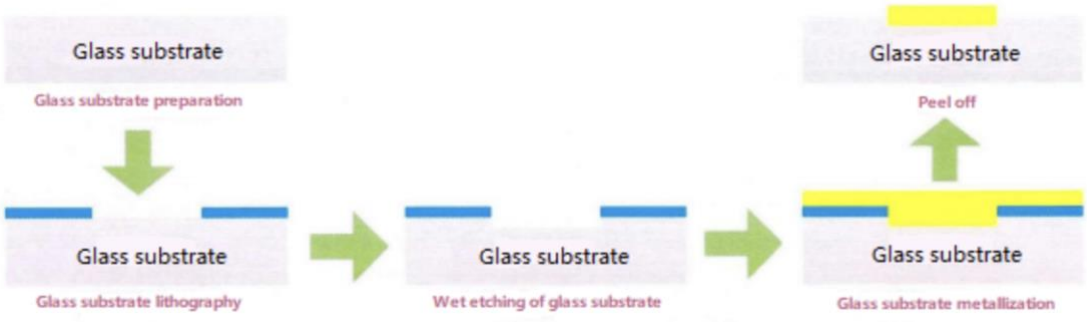

Fig. 1.16 Glass substrate fabrication process diagram.

Preparation of glass wafers:

1. Acetone and ethanol ultrasonic cleaning
2. Rinse with deionised water
3. Five minutes of hydrogen peroxide and sulphuric acid
4. Final rinse with deionised water

Photolithography on glass:

1. Photoresist coating (≥2 μm)
2. Bake for 15 minutes at 120°C

Wet etching (BHF) to create anchor points:

1. Buffered hydrofluoric acid etching at 45°C to a depth of 100 nm
2. Reaction: $SiO_2 + 6HF \rightarrow H_2SiOF_6$

Glass metal deposition:

Sequential sputtering of Ti/Pu/Au with thicknesses: 50 nm / 50 nm / 100 nm

Electrode patterning and lift-off procedure:

- Final ultrasonic cleaning and deionised water rinse
- The SOI wafer used has the following specifications:
- Diameter: 4 inches
- Structural layer: 70 μm
- Buried oxide (BOX) layer: 3 μm
- Handle (substrate) layer: 500 μm

Outlined below and depicted in Figure 1.17, the fabrication steps:

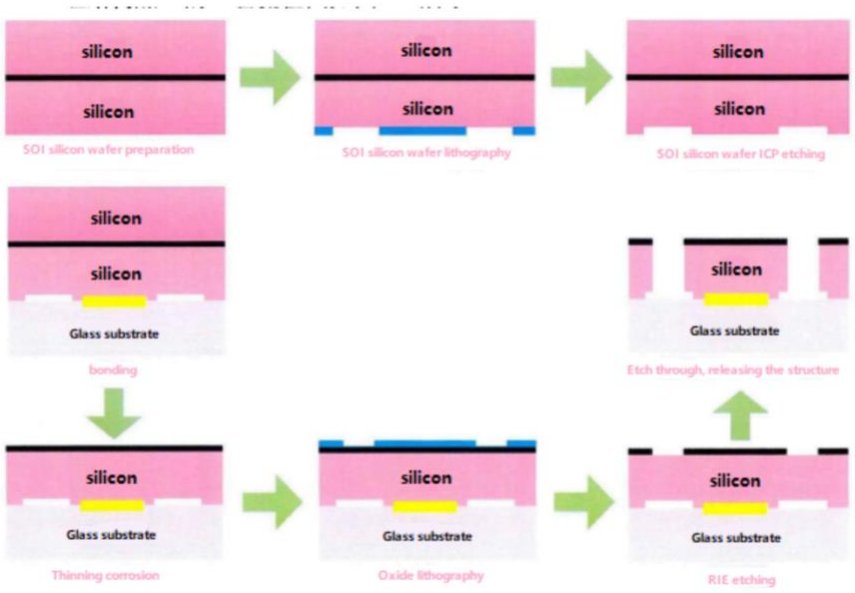

Fig. 1.17 SOI silicon structure fabrication flowchart.

1. Initial cleaning:

   Ultrasonic cleaning with acetone and ethanol

   Sulfuric acid and hydrogen peroxide cleaning

   Final rinse with deionised water

2. Lithography:

   Patterning on the device layer using photoresist ≥2 μm

3. Dry etching:

   Inductively Coupled Plasma (ICP) etching to 35 μm depth

4. Bonding:

   Glass-silicon bonding at 600 V, 300°C, and 300 mbar pressure

5. Wet etching of the substrate:

   Potassium hydroxide (KOH, 40%) at 80°C until oxide stop layer is reached

6. BOX layer lithography and alignment:

   Photoresist coating ≥2 μm and backside alignment

7. Oxide layer etching:

   Reactive Ion Etching (RIE) to a depth of 500 nm

   Photoresist removal

8. Final release:

Through-etching using ICP to release suspended structures (~55 μm depth)

Processing Challenges in SOI MEMS Fabrication

Though SOI-based techniques have many benefits, some restrictions and manufacturing mistakes can still compromise gyroscope performance.

Lithography quality and ICP etching accuracy are important determinants of structural correctness. Lateral over-etching (a deterministic error) and variances due to wafer flatness, curvature, or non-uniform photoresist exposure (random errors) can produce:

- Uneven comb finger spacing
- Inconsistent gaps between beams and proof masses
- Width variation in structural beams
- Centroid shift of the movable structure

Surface charge accumulation on silicon dioxide (Lag effect) in RIE etching can divert incoming ions towards the base of trenches, hence generating undesired footing or undercutting. This changes the centroid and resonance frequency of the gyroscopic structure, therefore producing variable behaviour among devices from the same wafer.

Other problems are:

- Residual tension at the bonding contact
- Mass imbalance after thinning or release
- Resonant frequency fluctuation among identical dies

Especially important in navigation-grade gyroscopes, these structural anomalies influence bias stability, sensitivity, and scale factor consistency.

1.4 Leading Manufacturers

A variety of worldwide producers spearhead the MEMS gyroscope market by means of sensor design, micro-fabrication, and system integration as they remain essential to contemporary navigation, motion tracking, and stabilisation systems. From ultra-compact sensors for mobile devices to high-stability gyroscopes for aerospace,

defence, and industrial navigation, these businesses cater to various performance levels.

From ultra-compact sensors for mobile devices to high-stability gyroscopes for aerospace, defence, and industrial navigation, these businesses cater to various performance levels.

Analog Devices, Inc. (USA)

Analog Devices (ADI) is one of the foremost suppliers of high-precision MEMS gyroscopes for tactical and industrial-grade applications. Renowned for their outstanding sensor stability and low noise, ADI's MEMS gyros are frequently included into IMUs (Inertial Measurement Units) employed in aerospace, robotics, and defence.

While the ADIS16470 and ADIS16490 families provide full multi-axis inertial systems with internal calibration and adjustment, their ADXRS series features single-axis gyros optimised for vibration conditions. In large industrial equipment where performance and long-term stability are important, ADI gyroscopes are preferred. Guided weaponry, UAV navigation, and autonomous vehicles all fall under this category.

Preferred in autonomous cars, UAV navigation, guided missiles, and heavy industrial equipment where performance and long-term stability are crucial, ADI gyroscopes are also used in other applications.

STMicroelectronics (EU)

A major provider of MEMS sensors for the automotive and consumer electronics sectors, STMicroelectronics Widely utilised in smartphones, wearables, game consoles, drones, and vehicle dynamic control systems, their MEMS gyroscopes are

Commonly included into mobile devices, the LSM6DSOX—an IMU integrating gyroscope and accelerometer—offers low power consumption, embedded machine learning, and good temperature stability. For high-volume applications needing compact form sizes and cost efficiency, ST's monolithic integration and low-footprint packaging have become popular options.

Bosch Sensortec (Germany)

A pioneer in MEMS sensor technology, Bosch has been instrumental in forming the consumer-grade inertial sensor sector. Their MEMS gyroscopes, like the BMI160 and BMI270, offer exact 3D motion tracking with low power consumption. Wearables, AR/VR systems, smart glasses, and IoT gadgets all include these sensors.

Bosch excels in highly integrated IMUs that provide sensor fusion with magnetometers and accelerometers, hence allowing complete orientation awareness in small devices.

TDK InvenSense (Japan/USA)

A major participant in the mobile and gaming sensor sector, InvenSense is now part of TDK. Combining gyroscopes with accelerometers and digital motion processors (DMPs), their MPU series—e.g., MPU-6050, MPU-9250, and ICM-42688-P—are among the most extensively used motion sensors worldwide.

Drones, cell phones, VR headsets, game controllers, and camera stabilisation devices all make great use of InvenSense MEMS gyros. Their low power consumption, real-time tracking, and excellent responsiveness make them perfect for battery-operated devices.

Murata Manufacturing Co., Ltd. (Japan)

Murata is particularly well-known for their small, low-drift MEMS gyroscopes used in automotive, medical, and industrial automation applications. Often utilised in their GyroStar® line, which offers great temperature stability and long-term dependability, often used in:

- Vehicle rollover detection systems
- Driver assistance systems (ADAS)
- Medical diagnostic equipment
- Robotics motion control

Murata's devices are made for exact angular velocity measurements and can function over great temperature ranges.

Ericco Inertial System (China)

Ericco focusses on navigation-grade, high-precision MEMS gyroscopes. Their solutions support sophisticated uses including tunnel navigation, directional drilling, north-finding devices, and autonomous cars.

Notable models:

- ER-MG2-50/100 with bias instability of 0.01–0.02 °/h
- ER-MG2-300/400 with bias instability of 0.03–0.05 °/h

Designed for strong performance in demanding environmental circumstances, including underground navigation and military-grade systems, these vacuum-sealed, thermally compensated devices are built to last.

ASC GmbH (Germany)

ASC provides precision inertial sensors comprising MEMS gyroscopes customised for aeronautical navigation, railway systems, wind tunnel testing, and automobile crash testing. Their sensors are meant to run under severe temperature and mechanical stress, and they produce low-noise outputs. Often included into mobile platforms and test equipment, ASC's adjustable MEMS solutions

Silicon Sensing Systems Ltd. (UK/Japan)

Using ring and tuning fork structures, Silicon Sensing Systems creates a range of MEMS gyroscopes and IMUs in a joint venture between Sumitomo Precision Products and Collins Aerospace. Their sensors are utilised in:

- Maritime and rail navigation
- Robotics and industrial automation
- Aerospace applications

Known for long-term bias stability and strong packaging for vibration-heavy settings, Silicon Sensing's CRG20 and DMU30 IMUs

Shenzhen Rion Technology Co., Ltd. (China)

Rion produces several MEMS-based inertial sensors for smart agriculture, vehicle control, navigation, and unmanned systems. With quick reaction times, high

shock resistance, and onboard temperature correction, these gyroscopes are fit for field and autonomous system use.

Nanjing Sky MEMS Co., Ltd. (China)

Sky MEMS offers inertial sensors designed for industrial robotics, oil drilling, geotechnical monitoring, and mining gear. Designed with tough casings, broad input voltage ranges, and resistance to electromagnetic interference, their MEMS gyroscopes.

Sensonor (Norway)

Focussing on tactical-grade MEMS gyroscopes like their STIM300 and STIM318 series, Sensonor provides ultra-low bias drift, high bandwidth, and exceptional temperature stability. These devices are used in precise navigation systems, missile systems, drones, and spacecraft. Sensonor specialises in keeping performance in dynamic settings with high vibration and high-G.

CHAPTER 2 MEMS GYRO BIAS

2.1 Definition of MEMS Gyro Bias

MEMS gyro bias refers to an unwanted output signal generated by a microelectromechanical system (MEMS) gyroscope. This signal occurs in the absence of true angular motion. A gyroscope output that is 0 in the absence of rotation in an ideal scenario is a malfunction. MEMS gyroscopes can produce a non-zero output signal even when completely stationary, due to various physical, electrical, and environmental factors. A non-zero output signal is called zero velocity or bias output.

Bias is the primary element of gyroscope inaccuracy, typically expressed in degrees per second (°/s) or radians per second (rad/s). Despite its appearance, bias is not a fixed variable; it can change over time and in response to external stimuli. Therefore, a more precise definition would indicate that it includes both static and dynamic elements:

Static Bias – a relatively constant offset that persists under stable environmental and operational conditions.

Bias instability - is defined as a change in bias that is both time-dependent and temperature-sensitive. This phenomenon is sometimes called bias drift. It is usually characterised as a stochastic process that is affected by internal sensor dynamics and aging processes.

Thermal bias - refers to the change in bias caused by changes in the internal or external temperature of a material, which affects the material properties and stress distribution.

Random Walk and Noise-Induced Bias – apparent bias variations caused by the accumulation of random noise components, particularly noticeable over longer periods.

Factors Affecting Bias

Biased MEMS gyroscopes are often explained by these factors.

1. Manufacturing Imperfections:
    - Structural asymmetry in the proof mass and frame
    - Non-uniform etching or residual stresses during fabrication
    - Misalignment of drive and sense axes
2. Electronic Circuitry:
    - Offset errors in amplifiers, analog-to-digital converters (ADC), and filters
    - Power supply fluctuations and thermal noise in integrated circuits
3. Mechanical Packaging and Stress:
    - Packaging-induced strain altering the resonant characteristics
    - Stress from solder joints, mounting, or PCB warping
4. Environmental Conditions:
    - Temperature gradients and changes
    - Mechanical vibration or acoustic interference
    - Long-term aging of mechanical and electronic components
    - Impact on System Performance

In inertial navigation systems (INS) and other applications that determine orientation by integrating angular velocity over time, bias poses a significant problem. Integration, as the act of aggregating all data, including errors and biases, results in a predicted angular error, called angular drift, that increases linearly with time. A bias of 0.1 degrees per second will lead to an error of 6 degrees after just one minute of operation if not corrected.

Therefore, bias must be detected, estimated, and corrected to achieve increased accuracy in applications such as:

- Aerospace navigation and control
- Autonomous vehicle localisation
- Robotic arm motion control
- Drone stability and orientation systems
- Tactical and strategic defence-grade inertial units

- Measurement and Modelling of Bias

MEMS gyro bias is commonly estimated using statistical signal analysis methods such as:

- Allan variance analysis – to separate deterministic and stochastic components of the signal
- Kalman filtering – to model and compensate time-varying bias in real-time systems
- Temperature calibration models – to account for thermally induced drift
- Polynomial or lookup table methods – for offline compensation using pre-characterised data

These techniques help distinguish between short-term noise and long-term bias behaviour, allowing for robust correction mechanisms.

2.2 Causes of Bias in MEMS Gyroscopes

MEMS vibrating gyroscopes, though compact and efficient, are highly sensitive to external and internal influences that lead to bias errors — undesired offsets in output even when no rotation is present. Physical, thermal, mechanical, and electrical elements cause these bias components, which undermine long-term stability and accuracy, particularly in dynamic or severe settings. Key sources of MEMS gyroscope bias are examined in this section utilising data from recent experimental and theoretical research.

Thermal Effects and Temperature-Induced Bias Drift

The performance of MEMS gyroscopes is greatly influenced by temperature. Even tiny changes in ambient or internal temperature cause notable differences in resonance frequencies, structural alignment, and output voltage levels. Much research verified that:

- Bias drift increases at elevated temperatures, often due to mismatched thermal expansion between the silicon structure, bonding materials, and packaging.
- A 1% mismatch between drive and sense frequencies can cause up to a 20% error in the output.

- Temperature fluctuations induce a change in the scale factor, bias instability, and signal noise.

$$\Delta Bias = \beta_T \cdot \Delta T \tag{2.1}$$

Where:

- $\Delta Bias$— Change in bias [°/s]
- β_T— Thermal coefficient of bias [°/s/°C]
- ΔT— Temperature change [°C]

Example:

If $\beta_T = 0.05$ °/s/°C and ΔT= 40°C, then:

$\Delta Bias = 2/$ s

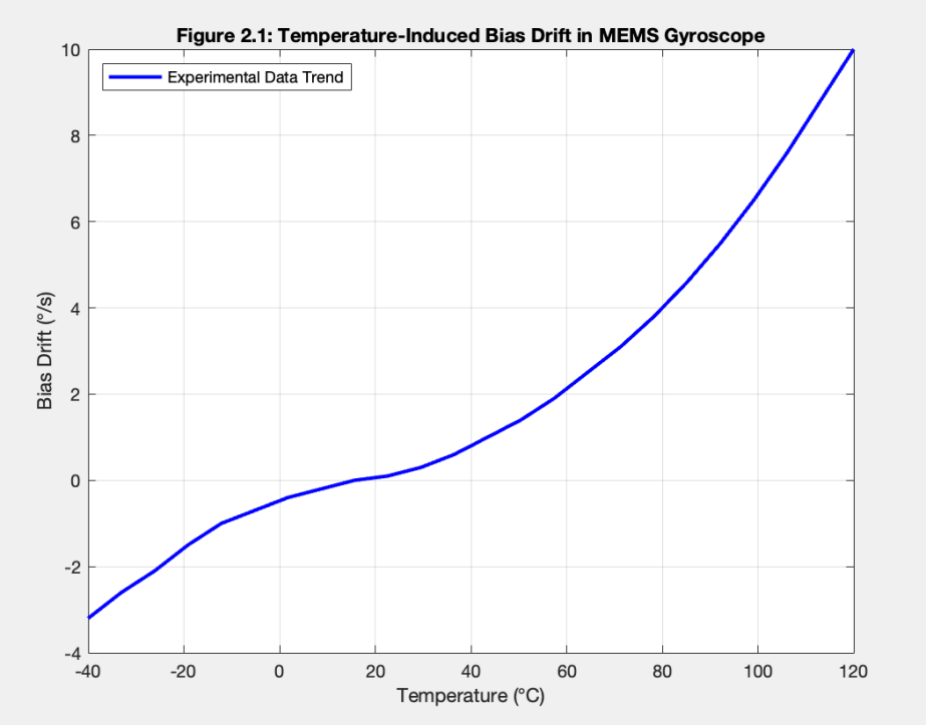

Fig. 2.1: Graph of bias drift vs. temperature showing exponential increase above 40 °C.

Mechanical Stress and Vibrations

Mechanical stress and high-intensity vibrations cause micro-deformations in the gyroscope structure that generate non-recoverable bias faults. These can come from:

- Environmental vibration fatigue

- Stress from PCB bending or package deformation
- Internal beam warping.

Bias drift of 1–1.8 °/s was found in experiments at high temperatures lasting more than 500 hours, especially in the last hours, suggesting that long-term mechanical wear is very important for bias growth.

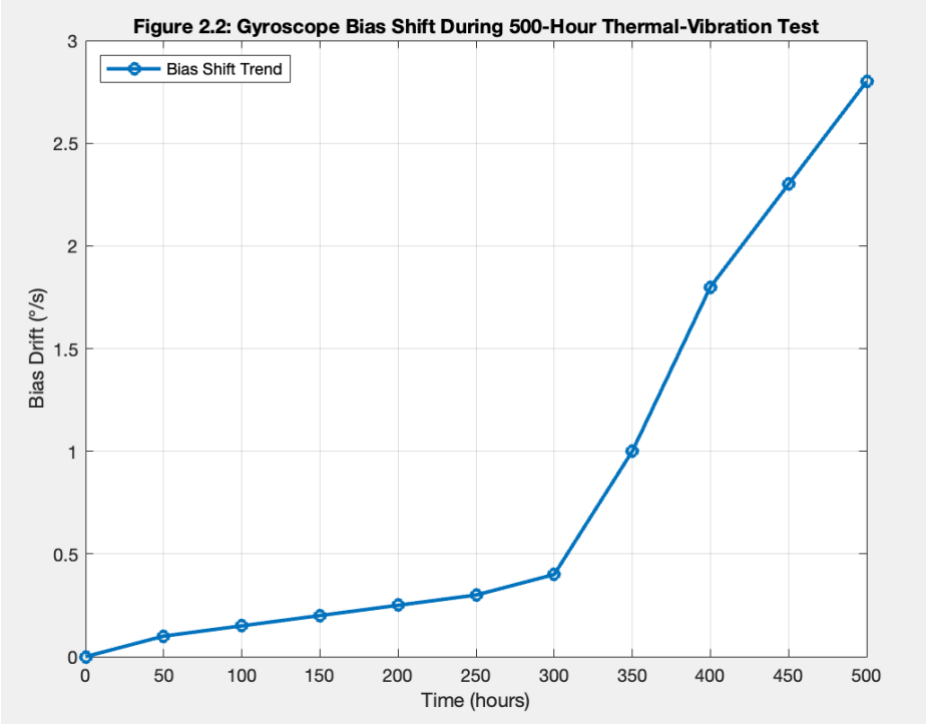

Fig. 2.2 Plot showing gyroscope bias shift during 500-hour thermal-vibration test.

Fabrication-Related Imperfections

Manufacturing inconsistencies such as sidewall angle errors, critical dimension variation, and misalignment of comb fingers introduce structural asymmetry. This leads to:

- Split resonant frequencies between drive and sense modes,
- Quadrature error,
- Inconsistent capacitance changes between cycles.

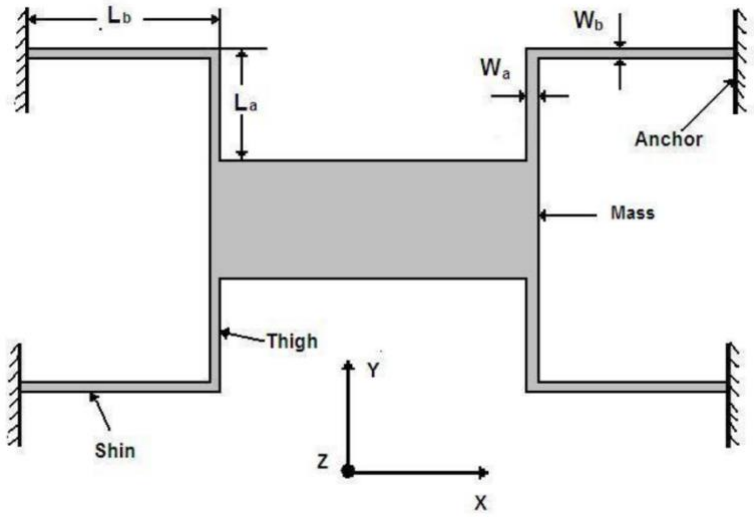

Fig. 2.3: Schematic of crab-leg suspension beam reducing deformation under temperature stress.

Outgassing and Packaging

Bad bonding between silicon and glass wafers creates leftover stress and possible vacuum leakage, which lowers the Q-factor of the gyroscope. Outgassing effects—caused by heat cycling or bonding interface flaws—lead to:

- Loss of vacuum seal
- Decreased sensitivity
- Increased bias fluctuation.

These problems were greatly lessened by a three-step vacuum wafer-level packaging technique (bake, interface optimisation, gold/titanium barrier), which was vital for long-term bias control.

Radiation and Electromagnetic Interference

Though less frequent in civilian uses, high-radiation settings (such as aerospace) produce lattice-level flaws in MEMS materials. These structural modifications immediately modify the oscillation behaviour and sensor accuracy, hence generating consistent or abrupt bias changes.

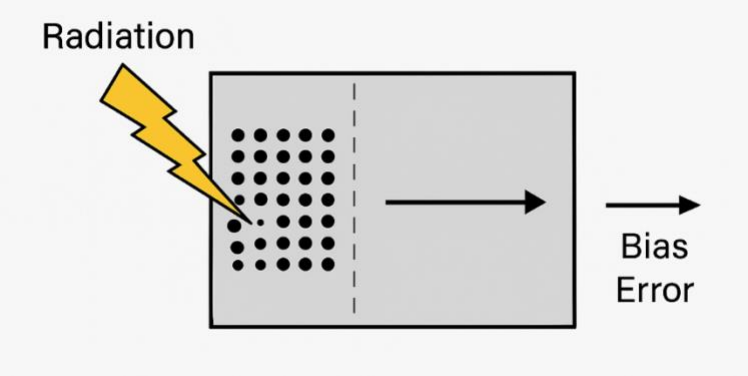

Fig. 2.4: Conceptual diagram: Radiation-induced lattice disruption causing bias error.

Mode Mismatches

Mode mismatch—the discrepancy between the inherent frequencies of the driving and sense modes—can potentially produce bias. This occurs due to:

- Fabrication tolerance limitations,
- Asymmetric suspension spring layout,
- Anisotropic material properties (like different Young's modulus in <110> vs. <100> silicon).

Experiments showed that lowering the resonant frequency split from 2 Hz to 0 Hz increased sensitivity by more than 3x and lowered bias instability from 5.4 deg/h to 0.96 deg/h.

Aging, Drift, and Long-Term Effects

With time, material fatigue, dielectric charging, and packing stress relaxation cause:

- Gradual drift in bias (slow and mostly irreversible).
- Creep in MEMS suspension structures.
- Signal offset change over hundreds to thousands of operational hours.

Though most started to show noticeable deterioration between 400 and 500 h with higher thermal cycling, several gyroscopes showed consistent performance up to 1000 h in controlled testing.

Mitigation Strategies and Research Trends

- Frequency-modulated (FM) gyroscopes with mode-decoupled architecture,

- Rate-integrating gyroscopes (RIGs) with anti-phase oscillations,
- Temperature-compensated packaging using titanium/gold layers,
- Closed-loop mode-matching control using PLLs or adaptive feedback loops.

Recent results showed:

- Temperature coefficients for bias dropped from 700 °/h/°C to ~3 °/h/°C,
- Long-term drift stabilised over 700+ hours of operation.

Table 2.1

Temperature Robustness of Advanced MEMS Gyroscope Designs

Year	Institution	Design	Temperature Range	Highlights
2012	Univ. of California, Irvine (USA)	Frequency-modulated	-40°C to +100°C	High Q-factors (~1 million) in both drive and sense modes.
2013	Univ. of California, Irvine (USA)	Whole-angle mode	+25°C to +35°C	Self-calibration of scale factor over 10°C range.
2018	Tohoku Univ., Sendai (Japan)	Frequency-modulated	+25°C to +75°C	Scale factor deviation: -52±136ppm/°C.
2018	Politecnico di Milano (Italy)	Frequency-modulated	+25°C to +70°C	Stable scale factor: ~35ppm/°C.
2020	Tohoku Univ., Sendai (Japan)	Rate-integrated	+25°C to +70°C	Excellent scale factor stability: -1.84±0.62ppm/°C.

Table 2.1 provides a comparative overview of frequency-modulated and rate-integrated MEMS gyroscopes, which demonstrate superior thermal robustness and reduced bias variability

2.3 Methods for Measuring Bias

Bias that can influence MEMS gyroscopes includes systematic error, stochastic drift, and environmental sensitivity, all of which provide more than simply a constant offset. Working on high-precision applications like navigation, robotics, or aerospace makes it essential to exactly identify this bias.

Below described are main methods for spotting bias as well as more theoretical and practical background knowledge.

Mean output (static average)

$$\mu = \frac{1}{N} \sum_{i=1}^{N} y_i \tag{2.2}$$

For a gyroscope, this is the average output value over time when the device is totally still. This approach presumes that all observable outputs are biassed since angular velocity should be zero.

Practicality:

- Bias estimate is fast and easy.
- It is often employed in self-calibration or real-time initialisation techniques.

It is perfect for low-processing embedded devices and electronics for consumers (phones and wearables). About limitation it is not dependable for long-term or high-accuracy systems and can't tell low-frequency noise or gradual drift bias. Although it should always be confirmed with a longer technique, this is perfect for quick testing or real-time uses.

Standard Deviation (Noise Assessment)

$$\sigma = \sqrt{\frac{1}{N-1} \sum_{i=1}^{N} (y_i - \mu)^2} \tag{2.3}$$

A statistical tool for measuring output spread around the mean, this helps to assess how "stable" the prejudice is. It decides if the bias estimate is constant, making it good for confidence intervals and system threshold filtering. It is perfect for confirming the consistency of results in static testing and is useful in sensor fusion with Kalman filter limiting. However, its disadvantage is that it just addresses the surrounding uncertainty and noise, not the bias itself. Advice: always contrast your bias reading with the mean to gauge its dependability.

Allan Variance / Allan Deviation

$$\sigma^2(\tau) = \frac{1}{2(M-1)} \sum_{k=1}^{M-1} \left(\overline{y}_{k+1} - \overline{y}_k\right)^2 \tag{2.4}$$

By examining its behaviour over several time scales, this method finds signal noise in the temporal domain. Plotting the Allan Deviation $\sigma(\tau)$ versus the mean time τ uncovers certain kinds of defects. Advantages: it distinguishes bias instability, white noise, rate random walk, and quantisation noise. Among both academics and manufacturers, this is the gold standard for sensor error modelling. Perfect for the aerospace industry, the military, satellites, and autonomous navigation systems, as well as developing sensor performance requirements. Caveats: data must be gathered over a long period of time—usually an hour or more—and it uses more computing power than average/standard processes. Use it to check sensor quality or conduct thorough performance study.

Bias Instability (From Allan Curve)

$$\textit{Bias Instability} = min\left[\sigma(\tau) \cdot \sqrt{ln(2)}\right] \tag{2.5}$$

The point at which the Allan deviation curve is flattest, suggesting the least degree of variance. Here, flicker noise, or irregular bias variation, takes the stage. Advantages: it provides a numerical value for the bias drift rate, usually expressed in degrees per hour or radians per hour. The manufacturer's specifications are directly comparable. The following conditions call for gyroscopes: long-term missions evaluating the performance of multiple MEMS sensors. Among its drawbacks are the

following: it just relates to computing Allan variance. It merely states the size; it does not clarify the cause of bias drift. Validating test results and contrasting commercial sensors depend much on this value.

Angular Random Walk (ARW)

$$ARW = \sigma(\tau) \cdot \sqrt{\tau} \tag{2.6}$$

In regions where white noise dominates, the slope of the Allan deviation curve is important. This indicates the short-term noise level of the gyroscope. Helps to define the sensor's resolution. Its help allows one to define the noise covariance of the Kalman filter. Suitable for systems needing rapid motion response, low-latency systems, drones, and fast robotics. Limitations: unhelpful for tracking long-term drift and misses environmental bias changes. Comprehensive error modelling should always accompany bias instability.

Histogram and Distribution Analysis

This graph method shows the probability distribution of sensor bias over time, indicating the frequency of static output values. Practical uses: aids in visualising whether the sensor's signal is distorted, steady, or multimodal. This can indicate hardware breakdown or abnormal behaviour. Suitable for examining flaws or age and testing to assess sensor quality. Caveats: requires interpretation. Unless curve fitting is applied, it does not generate a correct quantitative result. Suggestion: combine with Allan variance for visual evidence.

Table 2.2

Overview of MEMS Gyroscope Bias Determination Methods and Their Characteristics

Method	What It Measures	Best For	When to Use
Mean (μ)	Average offset	Quick bias estimation	Initialization, low-resource systems
Std. Dev. (σ)	Noise stability	Signal consistency check	Basic testing, filter tuning

Allan Variance	Time-domain noise decomposition	Long-term performance and drift analysis	High-end sensor validation, modelling
Bias Instability	Low-frequency drift component	Long-term bias error metric	Navigation, satellite, inertial systems
Angular Random Walk	Short-term white noise	Sensor resolution/noise floor	IMU design, Kalman filtering
Histogram Analysis	Output distribution shape	Visualizing bias variability	Debugging, failure detection, aging assessment

2.4 Mathematical Models of MEMS Gyro Bias

MEMS gyroscopes are miniature and very sensitive inertial sensors that transmute angular velocity into an electrical signal utilising the Coriolis effect. In actual application, however, their outcomes are often compromised by bias and noise stemming from internal deficiencies, external influences, and long-term drift. These extraneous factors must be mathematically represented for accurate correction, filtering, and system integration, as they undermine measurement precision.

In navigation and guidance systems, the integration of angular rate inputs leads to cumulative errors, making bias in MEMS gyroscopes particularly significant. Consequently, understanding, predicting, and alleviating these errors in hardware design and software processing rely on consistent mathematical modelling of bias.

Dynamic Physical Model of a Vibrating MEMS Gyroscope

A MEMS gyroscope consists of a vibrating mass-spring system where the Coriolis effect causes an out-of-plane displacement. The basic equations governing its motion are:

$$m\ddot{x} + C_x\dot{x} + k_x x = F_{drive}(t) \tag{2.7}$$

$$m\ddot{y} + C_y\dot{y} + k_y y = 2m\Omega\dot{x} \tag{2.8}$$

Here, the Coriolis force acts as the coupling term that shifts energy from the drive axis (x) to the sense axis (y) proportionally to the input angular rate Ω.

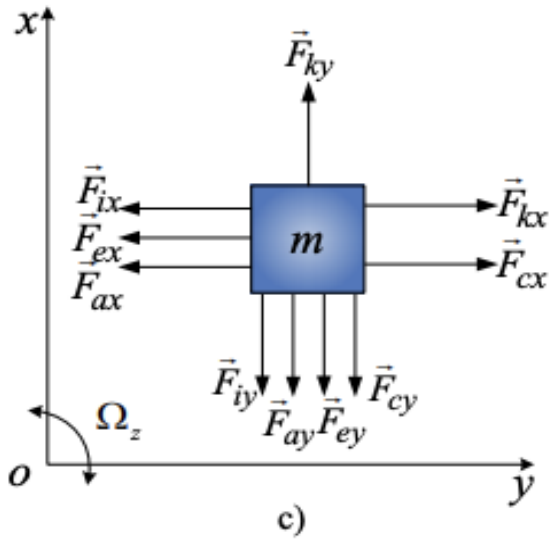

Fig. 2.6 Schematic representation of vibrating MEMS gyroscope showing excitation and sensing axes

Dimensionless and Simulation-Friendly Form

To simulate the system more efficiently, it's expressed using normalised parameters:

$$\ddot{x} + \frac{1}{Q_x}\dot{x} + \omega_x^2 x = \frac{F_{drive}(t)}{m} \tag{2.9}$$

$$\ddot{y} + \frac{1}{Q_y}\dot{y} + \omega_y^2 y = 2\Omega\dot{x} \tag{2.10}$$

Where Q_x, Q_y are quality factors and ω_x, $\omega_y$are natural frequencies.

These formulations help in modelling how the system responds over time, including how fast it settles, how it damps out vibrations, and what kind of errors (like bias) may remain.

Output Measurement and Bias Composition

The gyroscope's output is not just a clean angular rate but includes bias and noise:

$$\Omega_{measured}(t) = \Omega(t) + b(t) + n(t) \tag{2.11}$$

Decomposing Bias Components

Bias is not always constant. It evolves due to environmental or internal factors and can be modelled as:

$$b(t) = b_0 + b_T(T) + b_d(t) + b_w(t) \tag{2.12}$$

- b_0: static offset
- $b_T(T)$: temperature-dependent term
- $b_d(t)$: long-term deterministic drift
- $b_w(t)$: stochastic fluctuation (e.g., random walk)

Bias Stochastic Models

There are several models used for bias estimation in filters:

- Constant bias (good for short durations):

$$b(t) = b_0 \tag{2.13}$$

- Random walk:

$$b(t+1) = b(t) + \eta(t), \eta(t) \sim \mathcal{N}(0, q) \tag{2.14}$$

- First-order Gauss-Markov:

$$b(t+1) = \phi b(t) + \eta(t) \tag{2.15}$$

These models allow prediction of bias behaviour over time and are commonly implemented in Kalman filters for real-time correction.

Temperature-Induced Bias

Temperature changes can deform the structure or affect material properties, shifting the bias:

$$b_T(T) = \alpha(T - T_0) \tag{2.16}$$

Signal Demodulation and Output Processing

To extract meaningful angular rate data from physical displacement, the signal must be demodulated:

$$\Omega_{out}(t) = \frac{y_{demod}(t)}{K} \tag{2.17}$$

CHAPTER 3. ESTIMATION OF MEMS GYRO BIAS

3.1. Bias error model and Allan variance

A CVG output signal model equation expresses the relationship between the input and output of the gyroscope and can be represented in the following form:

$$U = (SF + \Delta SF)(\Omega + D) \tag{3.1}$$

where U is a CVG output signal in volts or digital code, SF is a CVG scale factor, ΔSF is a scale factor error, Ω is a measured angle rate, and D is a CVG bias drift.

A CVG bias drift is represented in the form:

$$D = D_B + D_E + D_R \tag{3.2}$$

where D_B is a bias, D_E is a drift depending on the environmental parameters, D_R is a random component of the CVG bias drift.

A bias D_B is a constant value that may change from switch-on to switch-on a gyro (i.e. maybe not repeatable) in a certain range of values.

The random component D_R of a bias drift contains many subcomponents. These subcomponents have different statistical characteristics. Therefore, when computing the angle of rotation, a CVG output signal is integrated (for example, when a gyroscope is used as part of a navigation system). In this case, these subcomponents will be accumulated at different rates, increasing the attitude measurement error. A subcomponent that accumulates faster than others should be maximally decreased at least up to other subcomponents' accumulation rates.

The quantitative determination of the subcomponents of a random drift should be made when a gyro is in a static position.

To determine values of random drift subcomponents, international standards [1-3] recommend using the Allan variation analysis for all modern gyroscopes, namely, ring laser gyroscopes, fiber optic gyroscopes and Coriolis vibratory gyroscopes including MEMS (vibratory) gyroscopes. The essence of this analysis is to build the plot of the dependence of the Allan variance on the averaging time by the measurement data.

Suppose that N successive values of the gyroscope output data were measured at a uniform time interval Δt. Then, clusters of n measurements in each one are formed, where $n < N/2$.

Each cluster contains data measured over time $T=n\Delta t$. Having denoted the instantaneous value of the gyroscope output signal as $\Omega(t)$, an average bias drift value over the cluster is determined as [2]:

$$\overline{\Omega}_{\mathrm{k}}(T) = \frac{1}{\mathrm{T}}\int_{t_k}^{t_k+T} \Omega(t)dt, \tag{3.3}$$

where $\overline{\Omega}_{\mathrm{k}}(T)$ is an average value of measurement data in the cluster that contains from k to $k+n$ data.

An average value over the next cluster is determined to be:

$$\overline{\Omega}_{\mathrm{k+1}}(T) = \frac{1}{\mathrm{T}}\int_{t_{k+1}}^{t_{k+1}+T} \Omega(t)dt\ , \tag{3.4}$$

where $t_{k+1}=t_k+T$.

Then, perform averaging for each cluster (the number of clusters is equal to N/n) is performed, and formed the differences:

$$\xi_{k+1,k} = \overline{\Omega}_{\mathrm{k+1}}(\mathrm{T}) - \overline{\Omega}_{\mathrm{k}}(\mathrm{T})\ . \tag{3.5}$$

The variance of the random sequence ξ determines the Allan variance for the averaging time, T, i.e.

$$\sigma^2(T) = \frac{1}{2T(N-2n)}\sum_{k=1}^{N-2n}\xi_{k+1,k}^2 = \frac{1}{2T(N-2n)}\sum_{k=1}^{N-2n}\left(\bar{\Omega}_{k+1}(T) - \bar{\Omega}_k(T)\right)^2. \tag{3.6}$$

The relative error δ of estimating the square root of Allan variance by expression (3.6) depends on the number n of measurements in the cluster of length $T=n\Delta t$ and is determined by the expression:

$$\delta = \frac{1}{\sqrt{2\left(\frac{N}{n}-1\right)}}. \tag{3.7}$$

From (3.7) it follows that to obtain the RMS of the Allan variance estimate error of 10% for the maximum cluster length, the minimum number of clusters must be 51. This means that if it is required to compute the Allan variance for the maximum time interval equal to T = 1 hour (with the RMS error no more than 10%), the minimum duration of the measurement data should be $N\Delta t$=51 hours. If the measurement data duration is less than 51 hours, then Allan variance estimate error for some last intervals will be more than 10%.

The Allan variance can also be determined for rate-integrating gyroscopes, the output signal of which is proportional to the angle of rotation:

$$\theta(t) = \int_0^t \Omega(\tau)d\tau \tag{3.8}$$

In this case, the following expressions are used:

$$\bar{\Omega}_k(T) = \frac{\theta_{k+n}-\theta_k}{T} \quad ; \quad \bar{\Omega}_{k+1}(T) = \frac{\theta_{k+2n}-\theta_{k+n}}{T}. \tag{3.9}$$

Now, considering expression (3.6) for the Allan variation of the output signal of a rate-integrating gyroscope, one can be obtained the following expression:

$$\sigma^2(T) = \frac{1}{2T^2(N-2n)}\sum_{k=1}^{N-2n}(\theta_{k+2n} - 2\theta_{k+n} + \theta_k)^2 . \tag{3.10}$$

Since Allan variance is a measure of a gyroscope's output signal stability, it must be related to the statistical characteristics of random processes that determine its performance.

There is a relationship between the Allan variance and the power spectral density of a random process [2].

$$\sigma^2(T) = 4\int_0^\infty S_\Omega(f)\frac{sin^4(\pi fT)}{(\pi fT)^2}df\ , \tag{3.11}$$

where $S_\Omega(f)$ is a power spectral density of a function $\Omega(T)$.

A graph of a function $\sigma^2(T)$ built by measurement data in log-log scale indicates a type of random component, which is in the gyro output signal. It is usually built a graph of a square root of the Allan variance $\sigma_\Omega(T)$ versus a length of time interval T (i.e. averaging time) on a log-log scale.

Different noise components appear on the Allan variance graph at different intervals of the averaging time variable T. This allows one to detect on the Allan curve various random components which are present in the measurement data. Assuming that the above noise components are independent of each other, the total Allan variance can be written as the sum of the variances of its components as follows [3]:

$$\sigma_\Omega^2(T) = \frac{3Q^2}{n^2T^2} + \frac{N^2}{nT} + \frac{2ln2}{\pi}B^2 + M^2\sqrt{\frac{nT}{3}} + K^2\frac{nT}{3} + R^2\frac{n^2T^2}{2} + \Omega_0^2\left(\frac{sin^2(2pf_0T)}{pf_0T}\right)^2 \tag{3.12}$$

A typical curve of the square root of Allan variance is shown in fig. 3.1.

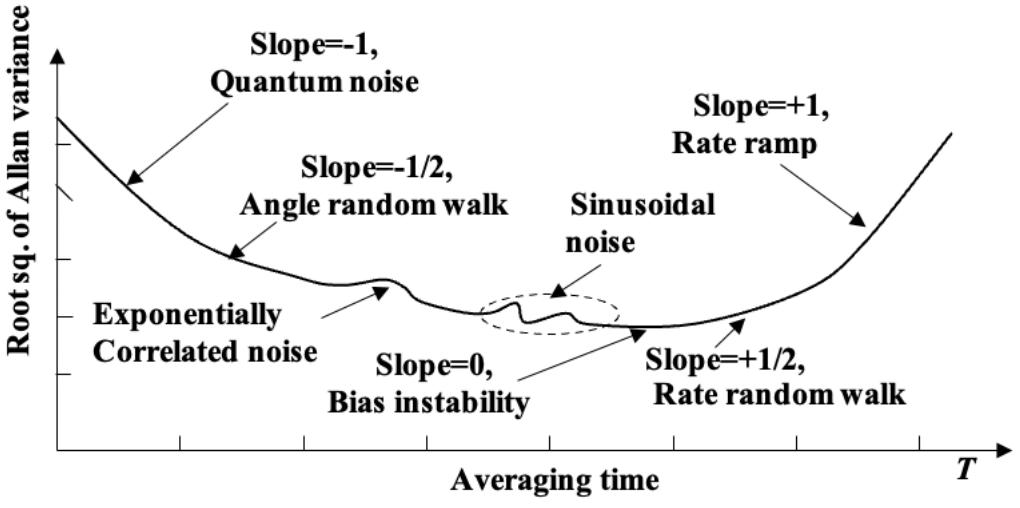

Fig. 3.1 Typical square root of the Allan variance versus averaging time

As can be seen from (3.12), the contribution of each subcomponent to total noise is quantitatively determined by corresponding coefficients Q, N, B, M, K, R, and Ω_0.

These coefficients are computed by the square root of the Allan variance graphed in log-log scale versus averaging time T such as described below.

Q is a random drift due to quantum noise measured in degrees (it is present only for digital gyroscopes); *N* is a random drift due to angle random walk measured in deg/h$^{1/2}$; *B* is a random drift due to bias instability measured in deg/h; *K* is a random drift due to rate random walk measured in deg/h$^{3/2}$; *R* is a random drift due to rate ramp measured in deg/h^2; *M* is a random drift due to exponentially correlated Markov noise measured in deg/h$^{3/2}$.

The *Q* value is determined as an ordinate of an intersection point of a tangential line with slope -1 (tanα=-1) to $\sigma_\Omega(T)$ curve and a vertical line originating from the point $T=3^{1/2}h$. It is measured in degrees. If $T_{max}<3^{1/2}$h, then $T=3^{1/2}s$ can be taken and, in this case, *Q* is measured in arcsec.

The *N* value is determined as an ordinate of an intersection point of a tangential line with a slope -0.5 (tanα=-0.5) to $\sigma_\Omega(T)$ curve and a vertical line originating from the point $T=1h$. It is measured in deg/h$^{1/}$2. If $T_{max}<1h$, then $T=1$ *s* can be taken and, in this case, *N* is measured in deg/h/Hz$^{1/2}$, deg/h$^{1/2}$=60 deg/h/Hz$^{1/2}$.

The *B* value is determined as an ordinate of a minimum of a $\sigma_\Omega(T)$ curve (it's flat part) divided by a constant $2\ln2/\pi\approx0.664$. It is measured in deg/h.

The *M* value is determined from the following equations [2]:

$$\sigma_\Omega(T_M) = 0.437\mathrm{M}\sqrt{T_c}\,;\; T_c = 1.89/\,T_M\,, \qquad (3.13)$$

where T_c is a correlation time of exponentially correlated noise, and T_M is an averaging time at which $\sigma_\Omega(T_M)$ is a local maximum of the convexity. The correlation function $C_M(t)$ of the exponentially correlated noise is $C_M(t) = Me^{t/T_c}$.

The *K* value of (3.12) is determined as an ordinate of an intersection point of a tangential line with a slope of 0.5 (tanα=-0.5) to $\sigma_\Omega(T)$ curve and a vertical line originating from the point $T=3\,h$. Its dimension is deg/h$^{3/2}$. If $T_{max}<3h$, then $T=3s$ can be taken and in this case, *K* dimension is deg/h/s$^{1/2}$, 60 deg/h$^{3/2}$= deg/h/s$^{1/2}$.

The *R* value of (3.12) is determined as an ordinate of an intersection point of a tangential line with a slope +1 (tanα=1) to $\sigma_\Omega(T)$ curve and a vertical line originating

from the point $T=2^{1/2}\ h$. It is measured in deg/h^2. If $T_{max}<2^{1/2}\ h$, then $T=2^{1/2}\ s$ can be taken and, in this case, R is measured in deg/h/s, 3600 deg/h^2=deg/h/s.

The Ω_0 value is determined from the following equations [2]:

$$\sigma_\Omega(T_s) = 0.725\Omega_0; \quad f_0 = 0.371/T_s, \tag{3.14}$$

where Ω_0 and f_0 are the amplitude and frequency of a sinusoidal noise, T_s is an averaging time at which $\sigma_\Omega(T_s)$ is a maximum (the first one) of the consecutive picks fall off rapidly in increasing of the averaging time T.

However, it is not necessary to present all components in the measurement data of the particular gyro.

3.2. Analysis of primary noise components for X-axis MEMS gyroscope of ADIS-16488 inertial measurement unit

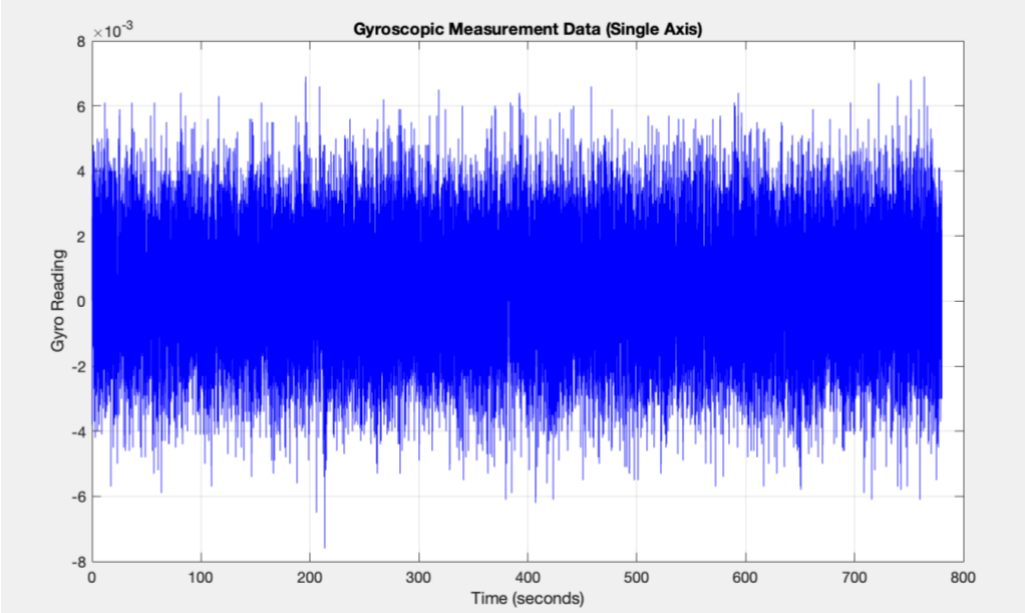

Fig. 3.2 Gyroscopic Measurement Data

Figure 3.2 shows bias versus time measurements of X-axis MEMS gyro of ADIS-16488 inertial measurement unit made by Analog Devices company (USA). Data was measured at room temperature when the gyro was at static position with sampling time Δt=0.02 s (50 Hz sampling frequency).

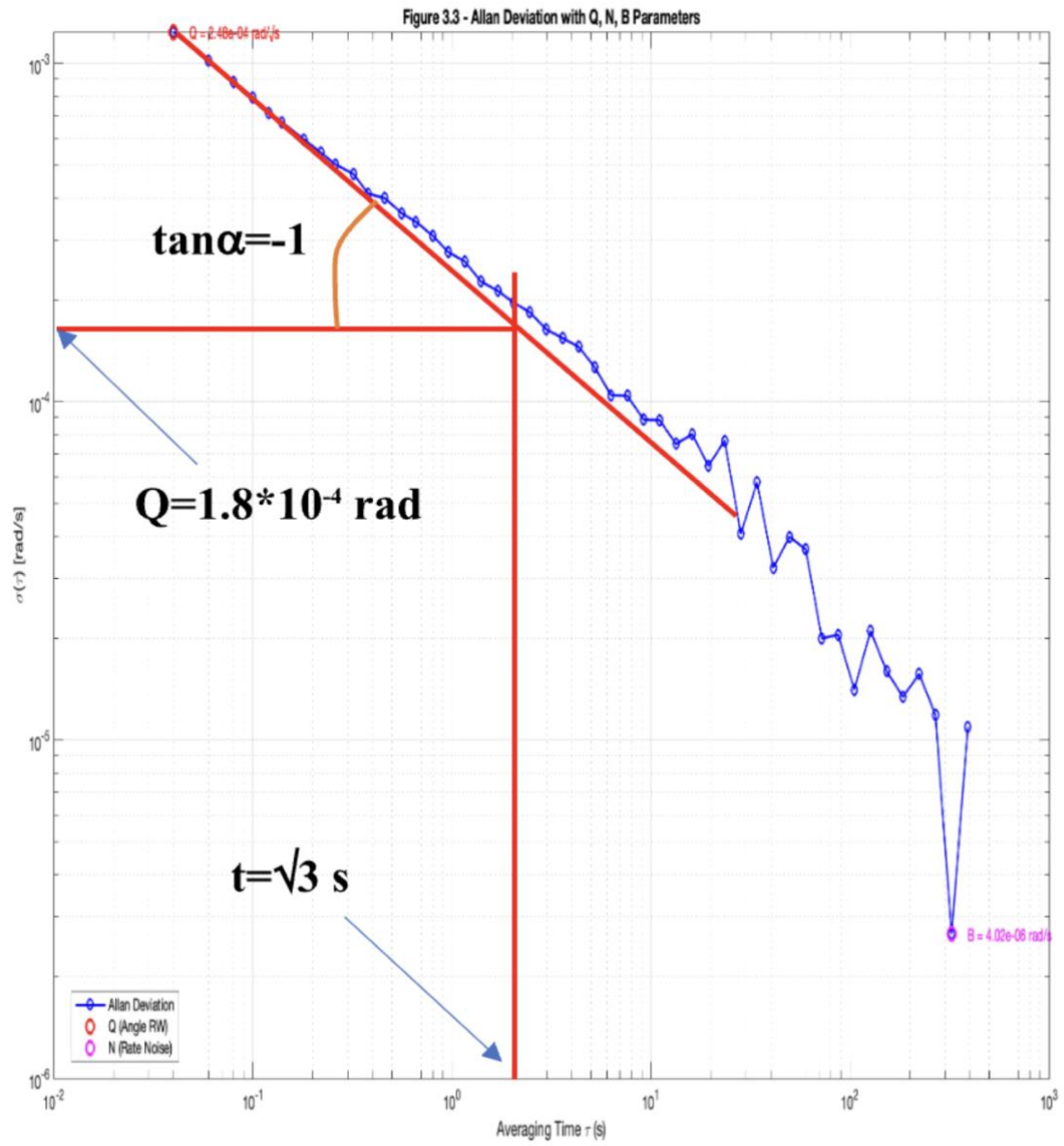

Fig. 3.3 Allan deviation curve with graphical identification of Quantization Noise (Q) parameter

This plot illustrates the Allan deviation $\sigma(\tau)$ as a function of averaging time τ, computed from static measurement data sampled at 50 Hz for the X-axis of the ADIS-16488 MEMS gyroscope. The red line segment with slope $\tan\alpha = -1$ corresponds to the region of quantization noise. According to standard methodology, the value of Q is determined at the intersection point where the tangent with slope -1 touches the Allan deviation curve, and the corresponding averaging time is $\tau = \sqrt{3}$ seconds. From the graphical construction, the value of the Q parameter was estimated as:

$$Q = \sigma(\tau) \cdot \sqrt{\tau} = 1.8 \times 10^{-4}\ \text{rad} \approx 0.01^{\circ}$$

This quantization noise reflects the white noise in the rate output of the gyroscope and is expressed in angular units — either radians, degrees, or arcseconds. It is a fundamental performance metric, particularly important in inertial navigation systems, as it influences the short-term integration error in angular displacement.

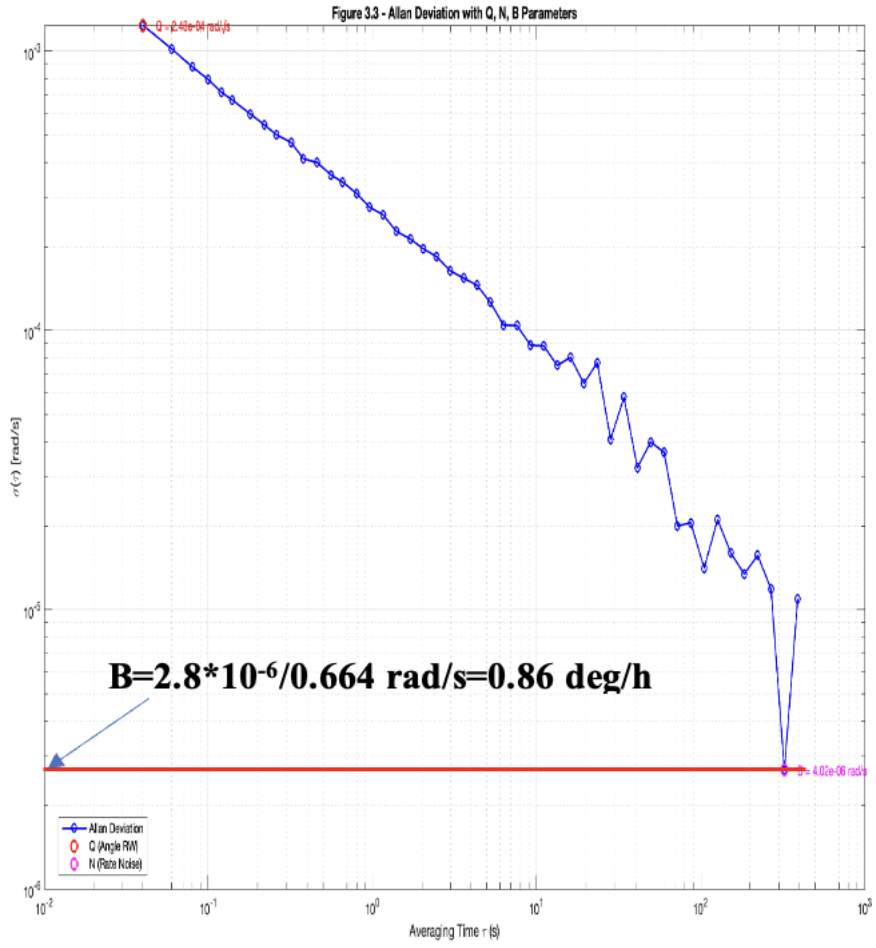

Fig. 3.4 Allan deviation curve with graphical identification of Bias Instability (B) parameter

The Bias Instability (B) component, associated with a flat region (slope ≈ 0) in the Allan deviation curve, was determined by locating the graphical minimum point of $\sigma(\tau)$. At this minimum, the Allan deviation value was measured as $\sigma_\tau = 2.8 \times 10^{-6}$ rad/s. According to formula (3.12), the bias instability is calculated as:

$$B = \frac{\sigma_\tau}{\sqrt{2\ln 2\,/\pi}} = \frac{2.8 \times 10^{-6}}{0.664} = 4.22 \times 10^{-6}\,\text{rad/s} = 2.4 \times 10^{-4}\,\text{deg/s}$$

$$\approx 0.86\,\text{deg/h}$$

This value characterizes the long-term drift in the sensor output, typically caused by environmental effects such as temperature changes, mechanical stress, and aging of internal components. Bias instability is one of the most important metrics for evaluating MEMS gyroscopes in high-precision applications like autonomous navigation, where GNSS signals may be unavailable.

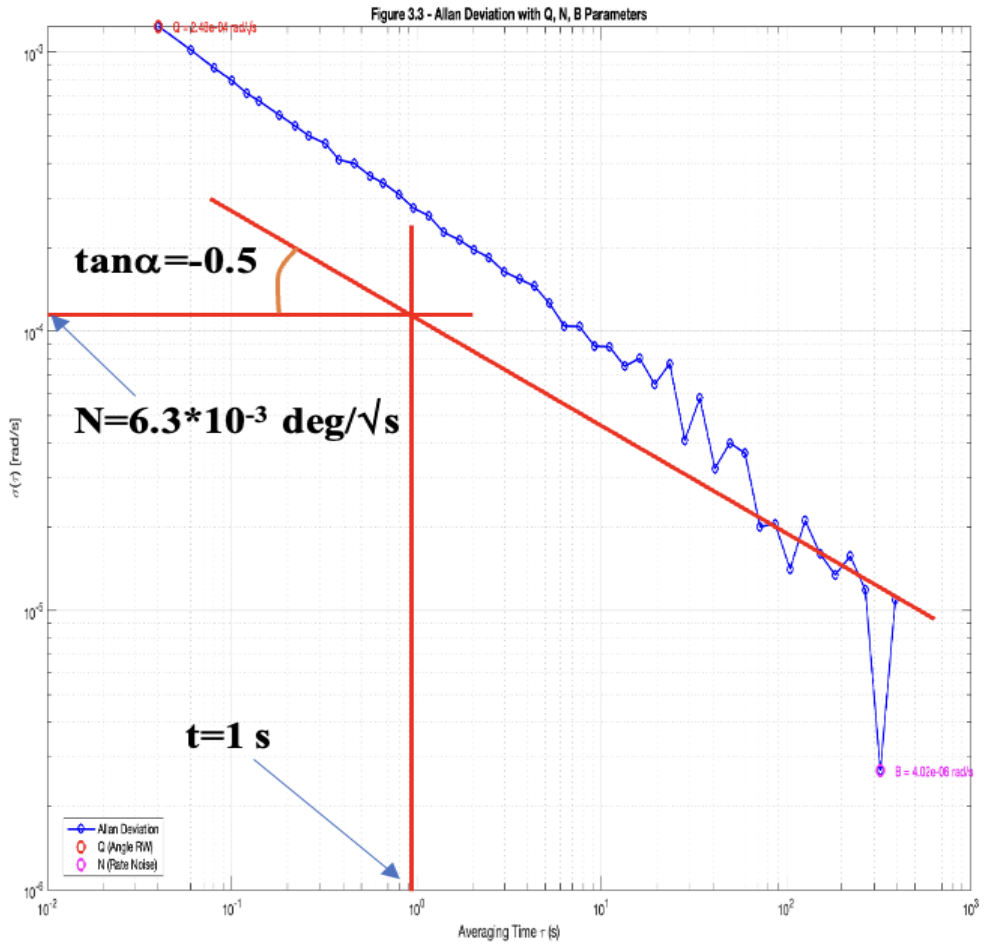

Fig. 3.5 Allan deviation curve with graphical identification of Angular Velocity Noise (N) parameter

The Angular Velocity Noise (N) component corresponds to a segment of the Allan deviation curve with a slope, which represents medium-frequency white noise in the angular rate signal. In this analysis, the region with slope $\tan\alpha = -0.5$ was graphically identified at an averaging time of $t = 1\,\mathrm{s}$. At this point, the Allan deviation was measured as $\sigma_\tau = 1.1 \times 10^{-4}\mathrm{rad/s} = 6.3 \times 10^{-3}\,\mathrm{deg/s}$.

According to the standard form of equation (3.12), the rate noise is expressed in units of deg/√s. Therefore:

$$N = \sigma_\tau = 6.3 \times 10^{-3}\,\mathrm{deg}/\sqrt{\mathrm{s}} \approx 0.38\,\mathrm{deg}/\sqrt{\mathrm{h}}$$

This parameter characterizes the spread of random variations in angular velocity due to sensor noise. It is relevant for systems where frequent small-angle changes can accumulate over time and affect control or navigation accuracy.

CONCLUSIONS

In the bachelor's qualification paper, a full-fledged study of the noise characteristics in the microelectromechanical (MEMS) gyroscope ADIS-16488 was performed using the Allan dispersion method. The study was based on the processing of real experimental data collected under static conditions in order to determine the key parameters that affect the accuracy and stability of measurements in gyroscopic sensors.

The work provides a detailed theoretical review of the nature of noise inherent in MEMS gyroscopes, as well as methods for their classification. The main attention is paid to such noise sources as angle random walk, bias instability, and angular velocity noise. These components, according to formula (3.12), have different temporal behaviour and appear in the Allan dispersion graph as areas with characteristic slopes on a logarithmic scale.

The practical part of the study was implemented by building a MATLAB program that allows for automated processing of gyroscopic data, plotting the Allan dispersion plot, and finding the values of the Q, B, and N parameters. The data were collected from the X axis of the ADIS-16488 gyroscope with a sampling frequency of 50 Hz, which allowed for more than 780 seconds of continuous measurement.

Based on the data processing, the following results were obtained:

- The value of the quantization noise (Q) is 1.8×10^{-4} rad, calculated at $\tau = \sqrt{3}$ s, which reflects the effect of digital resolution limits in the gyroscope output signal.
- The value of the bias instability (B) is 2.8×10^{-6} rad/s ≈ 0.86 deg/h, indicating the presence of low-frequency drift in the sensor output due to temperature variations, flicker noise, and long-term component aging.
- The value of the angular velocity noise (N) is 6.3×10^{-3} deg/$\sqrt{\text{s}}$ ≈ 0.38 deg/$\sqrt{\text{h}}$, which represents high-frequency white noise contributing to short-term fluctuations and integration error in angular velocity measurements.

Based on the performed analysis, the following conclusions can be drawn:

1. The Allan dispersion method is a universal tool for detecting and quantitatively analysing noise in inertial sensors. Its application allows for highly accurate assessment of the characteristics of MEMS gyroscopes even under limited testing conditions.

2. The developed MATLAB program is an effective and scalable tool for analysing gyroscopic data. It can be adapted to other types of sensors or to dynamic motion scenarios, which makes it useful in future studies.

3. The Allan dispersion graph, constructed based on gyroscope data, is an informative tool for assessing the quality of the sensor. It allows you to clearly determine the noise levels, compare the actual parameters with those typical for this class of devices, and also draw conclusions about the scope of its practical application.

4. The obtained results have applied value for autonomous navigation systems, robotics, aerospace engineering and instrument making. The parameters Q, N and B can be directly used in the development of error accumulation models, Kalman filters, or to estimate navigation drift in satellite-free conditions.

5. The proposed approach allows you to reduce dependence on external correction systems and provide more reliable positioning in closed or complex environments. This is especially relevant in the military sphere, in autonomous mobile systems and in the study of planetary surfaces.

6. The results of the work demonstrate the possibility of combining theoretical knowledge with practical engineering skills, in particular in the field of digital signal processing, mathematical modelling, programming and analysis of experimental data.

In general, the goal of the qualification paper has been fully achieved. The developed methods and obtained results can serve as the basis for further research in the field of inertial sensors, as well as find practical application in real engineering projects

REFERENCES

1. IEEE. *IEEE Standard Specification Format Guide and Test Procedure for Single-Axis Laser Gyros*. IEEE Std. 647-2006. IEEE Aerospace and Electronic Systems Society, 2006. 76 p. DOI: 10.1109/IEEESTD.2006.246241.

2. IEEE. *IEEE Standard Specification Format Guide and Test Procedure for Single-Axis Interferometric Fiber Optic Gyros*. IEEE Std. 952-1997 (R2003). IEEE Aerospace and Electronic Systems Society, 2003. 77 p.

3. IEEE. *IEEE Standard Specification Format Guide and Test Procedure for Coriolis Vibratory Gyros*. IEEE Std. 1431-2004. IEEE Aerospace and Electronic Systems Society, 2004. 69 p.

4. Effa D. *Design, Fabrication and Characterization of MEMS Gyroscopes Based on Frequency Modulation*. Master's Thesis. University of Waterloo, 2018. Available at: https://uwspace.uwaterloo.ca/items/e65fa7d6-3867-473d-8676-b4ee578c6726

5. Khan A., Wang J., Zhang Q., Wang C. A Noise Model for Gyroscope Signals Using EMD and Autocorrelation Function. *Journal of Intelligent Material Systems and Structures*, 2018, vol. 29, no. 6, pp. 1013–1024. DOI: 10.1177/1550147717746351. Available at: https://journals.sagepub.com/doi/pdf/10.1177/1550147717746351

6. Han S., Zhang Y., Wang M. Allan Variance Analysis for MEMS Gyroscopes. *Micromachines*, 2016, vol. 7, no. 2, article 195. DOI: 10.3390/mi7020195. Available at: https://www.mdpi.com/2072-666X/7/2/195

7. Wikipedia contributors. Vibrating Structure Gyroscope [Electronic resource] // *Wikipedia, The Free Encyclopedia*. Available at: https://en.wikipedia.org/wiki/Vibrating_structure_gyroscope (Accessed: May 12, 2025).

8. Gill W. A., Howard I., Mazhar I., McKee K. Micro-Electromechanical Systems Vibrating Gyroscopes. *Encyclopedia*, 2022. Entry ID: 29635. Available at: https://encyclopedia.pub/entry/29635 (Accessed: May 12, 2025).

9. Ericco Inertial Systems. Application of MEMS Gyroscopes in Navigation and Robotics [Electronic resource]. Available at: https://www.ericcointernational.com/application/mems-gyroscope-processing-technology.html (Accessed: May 12, 2025).

10. Metoree. MEMS Gyroscope Classification and Applications [Electronic resource]. Available at: https://us.metoree.com/categories/100148/ (Accessed: May 12, 2025).

11. El-Damak D., Bianchini J., Hu H., Zuo L. Analysis and Modeling of Gyroscope Noise. *IEEE Transactions on Instrumentation and Measurement*, 2014, vol. 63, no. 8, pp. 1944–1955. DOI: 10.1109/TIM.2014.2299971. Available at: https://ieeexplore.ieee.org/document/6703928

12. Gill W. A., Howard I., Mazhar I., McKee K. A Review of MEMS Vibrating Gyroscopes and Their Reliability Issues in Harsh Environments. *Sensors*, 2022, vol. 22, no. 19, article 7405. DOI: 10.3390/s22197405. Available at: https://www.mdpi.com/1424-8220/22/19/7405

13. National Center for Biotechnology Information. MEMS Gyroscopes: Review and Reliability [Electronic resource]. *PMC*, 2022. Article ID: PMC9571586. Available at: https://www.ncbi.nlm.nih.gov/pmc/articles/PMC9571586/ (Accessed: May 12, 2025).

```
%% Allan Variance Analysis for ADIS-16488 MEMS Gyroscope (X-axis)
% Author: Sofiia Melnychenko
% Based on formula (3.12), IEEE standards
% Extracting Q, N, B from Allan deviation

%% 1. Load Data
gyro = g1_16488(:);        % Ensure column vector

Fs = 50;                   % Sampling frequency in Hz
Ts = 1 / Fs;               % Sampling time (s)
N = length(gyro);          % Total number of samples

%% 2. Allan Deviation Calculation
maxM = floor(N/2);
m = unique(round(logspace(0.3, log10(maxM), 50)));  % averaging factors
tau = m * Ts;              % averaging times (T)
adev = zeros(size(tau));   % Allan deviation values

for i = 1:length(m)
    mi = m(i);
    L = floor(N / mi);       % number of clusters
    reshaped = reshape(gyro(1:mi*L), mi, L);
    y = mean(reshaped, 1);
    dy = diff(y);
    adev(i) = sqrt(0.5 * mean(dy.^2));
end

%% 3. Log-Log Slopes to Identify Noise Types
log_tau = log10(tau);
log_adev = log10(adev);
slopes = diff(log_adev) ./ diff(log_tau);

%% 4. Extract Q (Quantum noise ~ slope = -1) or ARW (slope = -0.5)
target_Q_slope = -0.5;
idx_Q = find(abs(slopes - target_Q_slope) < 0.05, 1);
T_Q = tau(idx_Q);
sigma_Q = adev(idx_Q);
Q = sigma_Q * sqrt(T_Q);          % Q in rad/√s

%% 5. Extract N (Rate Noise ~ slope = +0.5)
target_N_slope = 0.5;
idx_N = find(abs(slopes - target_N_slope) < 0.05, 1);
T_N = tau(idx_N);
sigma_N = adev(idx_N);
N = sigma_N / sqrt(T_N);          % N in rad/s/√Hz

%% 6. Extract B (Bias Instability ~ flat region)
[~, idx_B] = min(adev);           % minimum of Allan deviation curve
T_B = tau(idx_B);
sigma_B = adev(idx_B);
B = sigma_B / sqrt(2*log(2)/pi);   % B in rad/s

%% 7. Plot Allan Deviation + Q, N, B annotations
figure('Color','w');
loglog(tau, adev, 'b-o', 'LineWidth', 1.5);
grid on; grid minor;
xlabel('Averaging Time \tau (s)', 'FontSize', 12);
ylabel('\sigma(\tau) [rad/s]', 'FontSize', 12);
```

```
title('Figure 3.3 - Allan Deviation with Q, N, B Parameters', 'FontSize', 14);
set(gca, 'FontSize', 11);
hold on;

% Annotate Q
loglog(T_Q, sigma_Q, 'ro', 'MarkerSize', 8, 'LineWidth', 2);
text(T_Q*1.2, sigma_Q, sprintf('Q = %.2e rad/√s', Q), 'Color', 'r');

% Annotate N
loglog(T_N, sigma_N, 'go', 'MarkerSize', 8, 'LineWidth', 2);
text(T_N*1.2, sigma_N, sprintf('N = %.2e rad/s/√Hz', N), 'Color', 'g');

% Annotate B
loglog(T_B, sigma_B, 'mo', 'MarkerSize', 8, 'LineWidth', 2);
text(T_B*1.2, sigma_B, sprintf('B = %.2e rad/s', B), 'Color', 'm');

legend('Allan Deviation', 'Q (Angle RW)', 'N (Rate Noise)', 'B (Bias Instability)', 'Location', 'best');
hold off;

%% 8. Print Results (for report)
fprintf('--- Noise Parameters Based on Allan Deviation ---\n');
fprintf('Q = %.3e rad/√s (Angle Random Walk)\n', Q);
fprintf('N = %.3e rad/s/√Hz (Rate Noise)\n', N);
fprintf('B = %.3e rad/s (Bias Instability)\n', B);

% Convert B to deg/hour (optional for report)
B_degph = B * (180/pi) * 3600;
fprintf('B = %.3f deg/h\n', B_degph);
```